

Journal Pre-proofs

Research papers

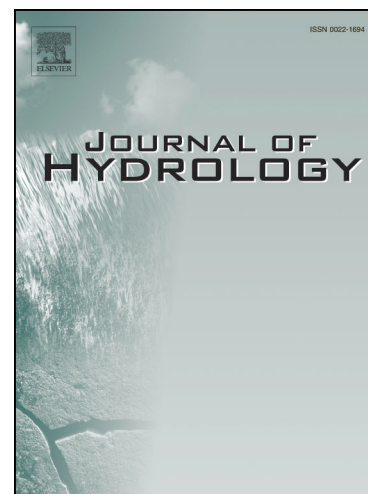
Delving into flash droughts in Vietnam during last two decades using the standardized evaporative stress ratio

Ngoc My Nguyen, Minha Choi

PII: S0022-1694(24)00063-5
DOI: <https://doi.org/10.1016/j.jhydrol.2024.130669>
Reference: HYDROL 130669

To appear in: *Journal of Hydrology*

Received Date: 7 June 2023
Revised Date: 30 October 2023
Accepted Date: 26 December 2023



Please cite this article as: Nguyen, N.M., Choi, M., Delving into flash droughts in Vietnam during last two decades using the standardized evaporative stress ratio, *Journal of Hydrology* (2024), doi: <https://doi.org/10.1016/j.jhydrol.2024.130669>

This is a PDF file of an article that has undergone enhancements after acceptance, such as the addition of a cover page and metadata, and formatting for readability, but it is not yet the definitive version of record. This version will undergo additional copyediting, typesetting and review before it is published in its final form, but we are providing this version to give early visibility of the article. Please note that, during the production process, errors may be discovered which could affect the content, and all legal disclaimers that apply to the journal pertain.

© 2024 Elsevier B.V. All rights reserved.

Delving into flash droughts in Vietnam during last two decades using the Standardized Evaporative Stress Ratio

Ngoc My Nguyen^{1,2} and Minha Choi^{3,4*}

¹School of Civil, Architectural, and Environmental System Engineering, Sungkyunkwan University, Suwon 440-746, Republic of Korea

²Department of Global Smart City, Sungkyunkwan University, Suwon 440-746, Republic of Korea

³School of Civil, Architectural Engineering and Landscape Architecture, Sungkyunkwan University, Suwon 440-746, Republic of Korea

⁴Department of Water Resources, Graduate School of Water Resources, Sungkyunkwan University, Suwon, 440-746, Republic of Korea

* Corresponding author

Professor

School of Civil, Architectural Engineering & Landscape Architecture, Sungkyunkwan University, 2066 Seobu-ro, Suwon, 16419, Republic of Korea

Tel: 82-31-290-7527

Fax: 82-31-290-7549

Email: mhchoi@skku.edu

1 Abstract

2 A flash drought is a recently defined extreme event that has destructive impacts on
3 agriculture as well as other elements of society and ecosystems. Understanding where and
4 when flash droughts occur can improve predictability and mitigation strategies for countries
5 with economies that rely on agriculture. This study represents the first investigation of flash
6 drought occurrences in Vietnam, one of the largest agricultural exporters in the world, using
7 the standardized evaporative stress ratio (SESR). Monthly SESR data captured historical
8 sustained drought events across the study period and exhibited a pattern similar to that shown
9 by the standardized precipitation evapotranspiration index over most of the study region, with
10 Pearson's correlations mostly ranging from 0.52 to 0.82. Results of the SESR analysis at a
11 pentad timescale indicate that flash droughts did occur in the country over the last two decades,
12 with the northern regions and a majority of the south-central coast experiencing fewer than 9
13 flash drought events that covered less than 20% of each region. The remaining southern areas
14 of the country were subjected to a much higher flash drought frequency, with 12 to 21
15 occurrences covering from 30% to more than 50% of the area in each region, typically during
16 the dry season and exacerbated by anomalies of potential evapotranspiration and temperature.
17 This research also revealed that flash droughts in Vietnam were correlated with the El Niño
18 Southern Oscillation climate phenomenon, particularly in the southern regions, where a high
19 flash drought frequency could take place under either El Niño or neutral conditions. This study
20 provides new evidence to support the development of a comprehensive overview of drought in
21 Vietnam, the country's drought mitigation strategies, and water management policies.

22

23 **Keywords:** Vietnam, flash drought, Standardized Evaporative Stress Ratio, ENSO.

24

25 1. Introduction

26 Droughts are among the most damaging natural hazards and an extreme phenomenon
27 worldwide (Smith and Katz, 2013) due to their detrimental effects on water supplies,
28 ecosystems, agricultural production, and society (Narasimhan and Srinivasan, 2005; Godfray
29 et al., 2010; Hu et al., 2019). Physically, a conventional drought event manifests as a prolonged
30 deficit in water storage and flux that can disrupt longstanding hydrological balances (Hobbins
31 et al., 2016). Notwithstanding the gradual and long-lasting features of traditional droughts, a
32 kind of drought event characterized by rapid intensification has been identified: a flash drought
33 (Hobbins et al., 2016; Wang et al., 2016; Forda and Labosier, 2017). Initially, a flash drought
34 occurs as a meteorological drought that can rapidly switch to an agricultural drought when
35 climatic conditions deteriorate; it is sometime termed an agricultural flash drought (Christian
36 et al., 2019). The speedy onset and evolution of drought is caused by severe atmospheric
37 anomalies, including the absence of rainfall, strong winds, high surface temperatures, and clear
38 skies, that last for several weeks. This combination of anomalies results in rapid land-surface
39 desiccation via excessive evaporative demand from the atmosphere regardless of prior moisture
40 conditions (Christian et al., 2019), significantly shortening the time available to mitigate the
41 impacts of drought (Otkin et al., 2015). A flash drought commonly has large effects on crop
42 yields, can result in economic losses (Hu et al., 2019; Li et al., 2020), and is likely to cause
43 greater agricultural and social devastation than evolving sustained droughts (Otkin et al., 2015).
44 As such, a better understanding of where and when flash droughts are likely to occur is needed

45 to improve the ability to predict them and implement mitigation strategies, particularly in
46 countries with economies dominated by agriculture.

47 As one of the world's largest agricultural exporters, Vietnam has a long history of
48 cultivation, one that has played a fundamental role in the rapid development of its economy
49 (Paul et al., 2004). Vietnam frequently suffers substantial economic losses due to droughts,
50 which are ranked third among costly natural hazards (Nguyen and Shaw, 2011). Quantifying
51 drought is therefore of paramount importance to the country. The nation's mainland is wholly
52 located in a tropical climate that is likely to experience severe droughts, particularly during El
53 Niño Southern Oscillation (ENSO) events (Lyon, 2004), and has high potential for flash
54 drought occurrence (Christian et al., 2021). Besides, along with the global warming, the mean
55 air temperature has been speedily increasing across Vietnam at a rate of 0.26 ± 0.10 °C per
56 decade since 1971, which is approximately twice the global rate for the same period (Nguyen
57 et al., 2014).

58 Despite widespread recognition of this threat, few studies (Zaki and Noda, 2022) have
59 examined the changes, probability, and frequency of droughts in Vietnam (Thanh et al., 2014;
60 Tue et al., 2015; Le et al., 2020, 2019). Those studies have improved understanding of drought
61 in Vietnam, but shortcomings and ambiguities in the research need to be clarified. For example,
62 most of these studies analyzed the evolution of meteorological droughts using a drought index
63 based only on precipitation (P) (i.e., the standardized precipitation index) (Thanh et al., 2014;
64 Tue et al., 2015), which can fail to capture the effects of warming on drought severity (Vicente-
65 Serrano, 2010). Thanh et al. (2014) applied drought indices based on a combination of P and
66 air temperature, such as Peday's and Martonne index. This work reflected the effect of global
67 warming on Vietnamese droughts, but these used drought indexes that may underestimate the
68 severity of extreme drought events because of a lack of information on the interactions between
69 soil moisture and evapotranspiration (Aghakouchak et al., 2014). Specifically, an indicator that
70 incorporates evapotranspiration, which plays a central role in energy-water exchange between
71 land surfaces and the atmosphere, would better track drought characteristics (Yao et al., 2010;
72 Kim and Rhee, 2016). Based on that understanding, Le et al. (2019) and Le et al. (2020) applied
73 the multivariate Palmer drought severity index and standardized precipitation
74 evapotranspiration index (SPEI), respectively, to assess drought conditions in Vietnam. Those
75 two indexes incorporate potential evapotranspiration (PET), as estimated by the Thornthwaite
76 equation, to reflect the involvement of warming in drought severity (Vicente-Serrano et al.
77 2010). However, a major debate about global drought trends has arisen due to the difference
78 between PET calculated by the Thornthwaite equation and those calculated by the Penman-
79 Monteith equations (Dai, 2012). Zhou et al. (2020) also pointed out that a temperature-based
80 method (i.e., the Thornthwaite equation) significantly underestimates PET, compared with the
81 output of other popular radiation-based (i.e., Priestley and Taylor) and energy balance-based
82 (Penmann–Monteith) methods, implying that drought indices that rely on Thornthwaite-
83 derived *PET* do not adequately capture the characteristics of drought extremes.

84 Previous studies concentrated on prolonged drought events, leaving a critical scientific
85 question unanswered: What are the characteristics of Vietnam flash droughts? With the
86 extreme devastation that flash droughts can cause to agricultural operations in mind, it is critical
87 to understand where and when flash drought events occur over the country. This research thus
88 attempts to answer that question and improve the country's capacity to predict flash droughts
89 and to develop mitigation strategies. Given that a drought can be viewed as 'flash' event when
90 moisture-stress conditions intensify rapidly (Otkin et al., 2018), a novel percentile-based
91 methodology proposed by Christian et al. (2019) relied on standardized evaporative stress ratio

92 (SESR) was used in this research due to its ability to comprehensively assess all the flash
93 drought criteria. In general, the main objective of this study is to pinpoint the characteristics of
94 flash drought in Vietnam by analyzing SESR-based drought index. This study attempts to
95 answer two main scientific questions:

96 (1) What are the characteristics of flash drought events in Vietnam?

97 (2) What is the relationship between ENSO and flash droughts in Vietnam?

98

99 2. Study area

100 Vietnam is a southeast Asian country on the Indochinese Peninsula, between 101.1 °E and
101 110.3 °E and 8.2 °N and 23.5 °N. Topographically, one-quarter of the country's territory is
102 covered by plains interspersed with hills and mountains. The remaining three-quarters are
103 mountains and hills that form an arc stretching from the northwest to the southeast of the
104 country and facing the East Sea. The north, south, and southwest of mainland are adjacent to
105 the East Sea. Vietnam has 3,260 km of coastline and thousands of islands and archipelagos.
106 The entire country has a tropical climate; the northern half has a tropical monsoon climate with
107 4 distinct seasons, and the southern half is a tropical monsoon with 2 seasons. For example,
108 northern Vietnam has a relatively cold winter, whereas the south experiences a warmer winter.
109 While the north experiences scorching temperatures in the summer, the south enjoys cooler
110 conditions. With a hot and humid climate, Vietnam has cultivated a prosperous agriculture
111 industry by devoting more than 70% of its land area to farming, making the country one of the
112 top rice producers in the world with many other agricultural products such as rice paddy, coffee,
113 soybeans, and corns.

114 Due to the complex topography and climatology of Vietnam, this study divided the country
115 into seven sub-regions: the North Mountains and Midlands (R1), Red River Delta (R2), North
116 Central Coast (R3), South Central Coast (R4), Central Highlands (R5), Southeast (R6), and
117 Mekong River Delta (R7), as shown in Fig. 1 and Table 1. Being under the influence of
118 monsoons and topography, two sub-regions, R1 and R2, have four distinct seasons yearly,
119 consisting of a dry and cold winter (from December to February), a tepid spring (from March
120 to May), a sweltering and humid summer (from June to August), and a mild autumn (from
121 September to December). Sub-region R3 has four seasons similar to those of the two northern
122 sub-regions, but experiences warmer temperatures during winter. All four southern sub-regions
123 have two seasons, including a dry season (from the end of November to April) and a rainy
124 season (from May to November). Coastal sub-regions R4 and R7 are hot year-round, whereas
125 both R5 and R6 experience cooler weather (Fig. 1). Overall, three sub-regions in the north
126 experience large variations among the seasons, with wide amplitudes of air temperature, while
127 four sub-regions in the south experience regularly hot weather with less fluctuation in air
128 temperature (Fig. 1). Using those differences in climatic conditions among regions, we
129 established the study at either regional or national mainland scales to investigate spatial-
130 temporal changes in flash drought events from 2003 to 2021.

131

132 3. Materials

133 3.1. Global Land Evaporation Amsterdam Model (GLEAM)

134 The GLEAM is a satellite-based global evapotranspiration dataset, providing adequate
135 information of actual evapotranspiration (AET), PET, and several other hydrological variables,
136 such as the components of land evapotranspiration and surface and root-zone soil moisture
137 (Miralles et al., 2011). This product was generated to maximize consolidation of satellite
138 observations and provide spatial-temporal continuity of terrestrial evapotranspiration at a
139 resolution of 0.25° on a daily scale. The model applies the Priestley and Taylor equation to
140 compute daily PET using surface available energy and air temperature, and then downscale
141 PET to AET using a dimensionless coefficient parameterizing the resistance to
142 evapotranspiration. The method might accurately calculate AET when compared with the well-
143 known Penmann-Monteith and Priestley-Taylor Jet Propulsion Laboratory approaches
144 (Miralles et al., 2016). In this study, the latest version 3.6b of GLEAM, which is based solely
145 on satellite data from January 1, 2003, to December 31, 2021, was downloaded to retrieve AET
146 and PET data. Then, GLEAM dataset covering mainland of Vietnam (7.8911°N to 23.3933°N
147 and 101.6250°E to 110.1250°E) was subset for using in this study.

148

149 3.2. Integrated Multi-satellite Retrievals for Global Precipitation Measurement

150 Global Precipitation Measurement (GPM) is a partnership between the US National
151 Aeronautics and Space Administration and the Japan Aerospace Exploration Agency that
152 provides global precipitation data at a high temporal and spatial resolution. The GPM level 3
153 product uses the Integrated Multi-satellite Retrievals for GPM (IMERG) system, which
154 incorporates all available precipitation data from ground-gauge analyses, microwave-
155 calibrated infrared data, satellite-microwave precipitation data, and other sources with half-
156 hourly temporal and $0.1^\circ \times 0.1^\circ$ spatial resolutions (Huffman, 2018). The IMERG system
157 generates three types of products: Early, Late, and Final runs, which have response times of 4
158 h, 12 h, and approximately 2 months, respectively, after observation (Huffman et al., 2020).
159 The Early and Late run types are conducted in near real-time and adjusted with climatological
160 coefficients that change by location and month. The Final run type is produced post-real-time
161 when gauge calibration is consistent with precipitation data supplied by the Global
162 Precipitation Climatology Centre. The Final run product is more accurate than other versions,
163 particularly over land, and is the most appropriate dataset for scientific research.

164 We used the Final run product of the latest IMERG (GPM_3IMERGDF_V06) to retrieve
165 P data for the study period. P for the mainland of Vietnam (7.8911°N to 23.3933°N and
166 101.6250°E to 110.1250°E) was the first subset, which was then upscaled to the pixel size of
167 the GLEAM data for further calculations. The temporal length of the P dataset was 3 months
168 shorter than the GLEAM dataset due to the time limit of IMERG products.

169

170 3.3. Climate indices

171 To examine the influence of ocean processes on drought events in Vietnam, popular
172 climatic indexes incorporating El Niño and La Niña events were used. The Oceanic Niño Index
173 (ONI), as defined by NOAA Climate Prediction Center, is a primary indicator that monitors
174 seasonal climate patterns over the ocean domain, namely ENSO. The ONI index tracks higher-
175 and lower-than-normal sea-surface temperatures in the east-central tropical Pacific Ocean
176 using running 3-month means. The Southern Oscillation Index (SOI) is one measurement of
177 large-scale air-pressure fluctuations, including El Niño and La Niña events, over the region

178 between the western and eastern tropical Pacific Ocean (Kiladis and van Loon, 1998). The SOI
 179 is standardized from observations of sea-level pressure to distinguish between the island nation
 180 of Tahiti and Darwin, Australia. Nino3.4 is a widely used index to define El Niño and La Niña
 181 episodes based on the average equatorial sea-surface temperature over a region stretching from
 182 the international dateline to the South American coast (Trenberth and Stepaniak, 2001). The
 183 multivariate ENSO index (MEI) is a temporal record of a leading combined empirical
 184 orthogonal function incorporating five key climatic variables (i.e., outgoing longwave radiation,
 185 sea-level pressure, sea-surface temperature, and the zonal and meridional components of
 186 surface winds) across the tropical Pacific basin (Wolter and Timlin, 1993; 1998). The trans-
 187 Niño index (TNI) quantifies the gradient in anomalies of sea-surface temperature between the
 188 central and eastern equatorial Pacific Ocean, which is measured as (Niño1 + 2) – (Niño4)
 189 (Trenberth and Stepaniak, 2001). These five climate indices were used to examine the
 190 association between ENSO modes and flash drought events in Vietnam. They can be download
 191 from <https://psl.noaa.gov/data/climateindices/list>, and include the study period (2003–2021).

192

193 4. Methodology

194 4.1. Standardized evaporative stress ratio drought index

195 4.1.1. Calculations

196 The SESR index was first proposed by Christian et al. (2019) to identify flash droughts by
 197 accounting for their fundamental drought features of a short duration and a large effect. SESR
 198 calculations contain AET and PET, both of which are highly sensitive to rapid changes in soil
 199 moisture and evaporative stress (ET_{stress}) in the atmosphere, and reflect the effects of radiation,
 200 humidity, temperature, and wind anomalies, all of which are involved in the intensification of
 201 flash droughts (Otkin et al., 2013). The SESR was computed using data from GLEAM, which
 202 provides an adequate and reliable dataset of daily AET, its components, PET, and soil moisture
 203 (Miralles et al., 2011). The SESR quantifies flash drought events using the concept of
 204 evaporative stress ratio (ESR) using AET and PET:

$$205 \quad ESR = \frac{AET}{PET} \quad (1)$$

206 where ESR varies within the range [0,1]. ESR values close to 0 indicate that moisture in the
 207 soil and vegetation meets little or none of the evaporative demand from the atmosphere. Values
 208 approaching 1 indicate that the available moisture on the land surface satisfies a majority or all
 209 of the evaporative demand from the atmosphere. Generally, the larger the ESR the lower the
 210 stress of evapotranspiration in the environment, and vice versa.

211 To avoid volatility in detecting flash drought events, the daily ESR were converted to a
 212 pentad scale (5-day mean) (Christian et al., 2019). Next, a standardized ESR was calculated
 213 from the pentad ESR to support comparisons of ET_{stress} among different regions and of ESR
 214 values over long time periods. The pentad ESR values were computed for each pixel as follows:

$$215 \quad SESR_{ijk} = \frac{ESR_{ijk} - \overline{ESR_{ijk}}}{\sigma_{ESR_{ijk}}} \quad (2)$$

216 where $SESR_{ijk}$ is the z -score of ESR for a specific pixel (i,j) at the time of pentad k and \overline{ESR}_{ijk}
 217 and $\sigma_{ESR_{ijk}}$ are the mean and standard deviation, respectively, of ESR at a specific pixel (i,j)
 218 and the time of pentad k for all available years during the study period.

219 To identify the ‘flash’ characteristic of drought, the pentad-to-pentad change of SESR
 220 ($\Delta SESR$) was calculated at each pixel over the study duration. These changes were standardized
 221 in the same manner:

$$222 \quad (\Delta SESR_{ijk})_z = \frac{\Delta SESR_{ijk} - \overline{\Delta SESR}_{ijk}}{\sigma_{\Delta SESR_{ijk}}} \quad (3)$$

223 where $(\Delta SESR_{ijk})_z$ is the z -score of the change in the SESR for a specific pixel (i,j) at the time
 224 of pentad k , and $\overline{\Delta SESR}_{ijk}$ and $\sigma_{\Delta SESR_{ijk}}$ are the mean and standard deviation of the SESR
 225 changes, respectively, at a specific pixel (i,j) and the time of pentad k for all available years
 226 during the study period.

227

228 **4.1.2. Flash drought detection**

229 To define whether a drought qualifies as ‘flash’ event, four criteria were thoroughly
 230 evaluated based on the SESR and $\Delta SESR$ at each pixel, following [Christian et al. \(2019\)](#):

- 231 (1) The declining SESR must last for at least six pentads, equivalent to five $\Delta SESR$.
 232 (2) The final SESR value of the duration should fall below the 20th percentile of the SESR.
 233 (3) The third criterion includes two components: (3a) $\Delta SESR$ should be equal to or less
 234 than the inter-pentad 40th percentile value; and (3b) only one $\Delta SESR$ is allowed to be larger
 235 than 40th percentile value following a $\Delta SESR$ that satisfies criterion 3a. When criterion 3b is
 236 met, the following $\Delta SESR$ must reach criterion 3a and have a final $\Delta SESR$ of a flash drought
 237 event smaller than the SESR value of the two previous pentads.
 238 (4) The mean value of $\Delta SESR$ over the entire flash drought duration must be under the
 239 threshold of the 25th percentile value of the climatological changes in SESR at that pixel and
 240 time of year.

241 The percentile thresholds used in criteria 2 and 3 were retrieved from the data variability
 242 of SESR and $\Delta SESR$ for each local pixel and specific pentad of all years during study period.
 243 The percentile thresholds applied in criteria 4 were computed using the $\Delta SESR$ for all pentads
 244 of a flash drought event at a local pixel level.

245

246 **4.2. Standardized precipitation evapotranspiration index (SPEI)**

247 To evaluate the SESR performance, PET data from GLEAM products were utilized not
 248 only to compute the SESR but also to replace the Thornthwaite-based PET in the SPEI

249 calculations in current work. Because PET in GLEAM products was retrieved using
 250 observations of near-surface air temperature and surface net radiation based on the Priestley
 251 and Taylor algorithms (Miralles et al., 2011), which efficiently calculate PET values similar to
 252 those generated by the Penmann–Monteith method (Zhou et al., 2020). The SPEI was selected
 253 for comparison because it is simpler than the Palmer drought severity index (Vicente-Serrano,
 254 2010), and superior to the Standardized Precipitation Index in taking warming into account
 255 when quantifying drought severity (Beguería et al., 2014).

256 By definition, the SPEI is based on the climatic water balance, known as the difference
 257 between P and PET. We computed the SPEI following a procedure described by Vicente-
 258 Serrano (2010) with two main steps:

259 (1) The accumulation of water deficit D_w ($D_w = P - PET$) was calculated at 1-month
 260 timescales for each pixel to better examine seasonal drought variations.

261 (2) To obtain the SPEI, D_w was normalized into a log-logistic probability distribution using
 262 two equations:

$$263 \quad F_{(\chi)} = \left[1 + \left(\frac{\alpha}{\chi - \gamma} \right)^\beta \right]^{-1} \quad (4)$$

$$264 \quad SPEI = W - \frac{c_0 + c_1 W + c_2 W^2}{1 + d_1 W + d_2 W^2 + d_3 W^3} \quad (5)$$

265 Where $F_{(\chi)}$ is the probability distribution function of variable D_w , and α , γ , and β are the
 266 respective scale, origin parameters, and shape of the log-logistic distribution (Vicente-Serrano,
 267 2010; Yao et al., 2018). With $P(D_w) \leq 0.5$, $W = \sqrt{-2 \ln(P(D_w))}$, where $P(D_w) = 1 - F(\chi)$; with
 268 $P(D_w) \geq 0.5$, $(1 - P(D_w))$ is used instead of $P(D_w)$ and the sign of the SPEI is reversed.

269

270 4.3. Other examining methods

271 4.3.1. Statistical analyses

272 The modified Mann–Kendall (MMK) trend test (Hamed and Rao, 1998) and Sen’s slope
 273 (Sen, 1968) were used to examine trends in precipitation, ET_{stress} (which measures differences
 274 between PET and AET), and flash drought conditions in the study regions. The MMK test,
 275 which statistically evaluates the monotonic trends of hydrological variables over time, was
 276 selected because it is a widely used non-parametric test with low requirements for data
 277 distribution and quality. The robustness of the MMK test allows it to consider the effects of
 278 autocorrelated time series that can affect trend results (Hamed and Rao, 1998). Sen’s slope,
 279 which is also a well-known non-parametric method, was chosen because it is not sensitive to
 280 outliers and is regularly applied to assess trends in univariate meteorological and hydrological
 281 time series (Hamed, 2009; Gocic and Trajkovic, 2013). We conducted an inter-comparison of
 282 the SESR and SPEI and an examination of the linkage between those drought indexes and
 283 ENSO phases at each grid point within the study region using Pearson’s correlation (R). Values

284 of R range within $[-1,1]$, with a larger R representing a higher correlation between these two
 285 indices and vice versa (Nguyen and Choi, 2022).

286

287 4.3.2. Features of drought dynamics

288 Temporal and spatial patterns of flash drought were examined using frequency of
 289 occurrence (f_D) and drought area percentages (PDA), respectively (Le et al., 2020). f_D and PDA
 290 are calculated using the following equations:

$$291 \quad f_D = \frac{\sum_{j=1}^n Du_j}{N} \times 100\% \quad (6)$$

292 where Du_j is the j th flash drought duration detected using frameworks described in Section
 293 4.1.2; n is the total number flash drought duration at a specific pixel, and N is the number of
 294 pentads during study periods, and

$$295 \quad PDA_{(m)} = \frac{A_{DA}}{A_{Total}} \times 100\% \quad (7)$$

296 where A_{DA} is the number of pixels with flash drought conditions and A_{Total} is the total number
 297 of pixels within the regions.

298

299 5. Results and discussion

300 5.1. Characteristic of climate over seven sub-regions

301 5.1.1 Annual variation of P and ET_{stress}

302 To the best of our knowledge, no previous studies have focused on ET_{stress} in the
 303 atmosphere in Vietnam despite the fact that the climate features across southeast Asia are
 304 strongly affected by the annual change in surface-atmosphere circulation (Le et al., 2019). This
 305 section examines annual variability not only in P but also in ET_{stress} , estimated as the difference
 306 between PET and AET ($PET - AET$), as shown in Fig. 2.

307 The annual patterns of both P and ET_{stress} differ between the northern and southern regions.
 308 The northern regions (R1–3) generally have relatively high P magnitudes (nearly 200 to 500
 309 mm month⁻¹) from May (the end of spring) to October (the middle of the fall), whereas the
 310 rainy months in the southern regions (R4–7) last longer, from May to November, but with
 311 lower amounts (nearly 200 to 400 mm month⁻¹) during peak time. The dry period of regions
 312 R1–3 lasts from November (the end of fall) to April (the middle of spring) with little P (from
 313 20 to 80 mm month⁻¹), during winter, when P is below 40 mm month⁻¹. The dry season in
 314 regions R4–7 (December to April) showed slightly higher P (mostly above 40 to more than 100
 315 mm month⁻¹) compared with (R1–3) during same period. ET_{stress} is small in regions R1–3
 316 (mostly below 10 mm month⁻¹) and increases toward regions R4–R7 (reaching nearly 70 mm
 317 month⁻¹ in R7), with distinct patterns in annual change. Region R1 showed lower ET_{stress}

318 compared with R2 and R3, where small ET_{stress} values were common during winter and spring,
 319 and an insignificant ET_{stress} (close to 0) was seen during summer and fall. ET_{stress} in region R2
 320 randomly fluctuated during the one-year course, but remained relatively large, at nearly 10 mm
 321 $month^{-1}$ during winter (January to March), with a low P or during summer (June and July), with
 322 a large P amount. In R3, ET_{stress} had a similar increasing tendency with P, which started in
 323 winter and reached a peak of approximately 12 mm $month^{-1}$ in the hot summer (June and July),
 324 but ET_{stress} then steadily declined during the peak of the rainy months (August and September).
 325 All four southern regions (R4–7) had much higher ET_{stress} during the dry season, in which the
 326 south-central region (R4 and R5) has approximately 40 mm $month^{-1}$ of ET_{stress} and the southeast
 327 regions (R6 and R7) approached 70 mm $month^{-1}$ of ET_{stress} at peak time. After peak time, ET_{stress}
 328 in R4 gradually decreased when the rainy season began and hit bottom in October, while ET_{stress}
 329 in R5–7 rapidly declined immediately after the onset of the rainy season. A significant
 330 intensification of ET_{stress} was observed in R7, beginning in July, under rainy weather. Overall,
 331 the northern regions (R1–3) annually have much wetter conditions than do the southern regions
 332 (R4–7). While moisture deficit in R1–3 may occur either in the cold (and dry) season (R1 and
 333 R2) or in the hot (and rainy) season (R2 and R3), the southern R4 and R5 regions mostly
 334 experienced an extreme surface dryness during the dry season. One feature in common between
 335 the R3 and R4 central coast regions is that, during hot conditions, the moisture deficit is not
 336 robustly sensitive to P, with steady increases (R3) and decreases (R4) expected with rainfall
 337 escalations.

338 Compared with regions R4–7, regions R1–3 experienced a larger amplitude of air
 339 temperature (Fig. 1) that varied seasonally in a pattern that matched that of P (Le et al., 2019).
 340 Lower air temperatures during the winter may generate a small evaporative demand in the
 341 atmosphere (Donohue et al., 2010) regardless of low P conditions, and high P may supply water
 342 for extreme evaporative demand caused by scorching hot temperatures during summer.
 343 However, ET_{stress} may still occur during the sultry summer despite relative rainy conditions in
 344 R2 and R3, and in R3 in particular, revealing the potential for droughts to occur in these regions
 345 under such weather. In southern regions R4–7, the massive ET_{stress} during the dry season was
 346 due primarily to its significantly low P and constantly high air temperature, particularly in R7,
 347 which had the highest mean temperature (Fig. 1) in the country. In addition, the increasing
 348 trend in ET_{stress} magnitude from the northern R1 region toward the southern R7 region was
 349 similar to trends in mean temperature across the stations in the seven sub-regions (Fig. 1),
 350 suggesting a dependence of ET_{stress} on air temperature rather than on P in study region. Among
 351 the regions, R1 commonly experienced lower air temperatures than R2 and R3, which can be
 352 attributed to the effects of the high elevations of this region (Fig. 1) (Le et al., 2019); ET_{stress} in
 353 R1 was correspondingly lower than in R2 and R3. Although it was within the rainy months,
 354 ET_{stress} in R3–4 still showed a steady change due to steep terrain and narrow hills, which have
 355 minimal water-holding capacity, resulting in a moisture deficit in the regions. Overall, these
 356 findings indicate that ET_{stress} was much higher in the southern R4–7 regions than in the northern
 357 R1–3 regions, particularly during the dry months. ET_{stress} conditions in Vietnam are generally
 358 not strongly disturbed by P due to the hot weather and complex topography of the country,
 359 which potentially leads to differences in drought quantification between P-based and ET-based
 360 indexes.

361

362 5.1.2 Inter-annual variation of P and ET_{stress}

363 To further examine the long-term trends in P and ET_{stress} , results of MMK tests, illustrated
 364 as spatial maps in Fig. 3 and Fig. 4, were used to describe inter-annual and inter-seasonal
 365 tendencies and slopes, respectively, during the study period.

366 At an inter-annual time scale, MMK analysis revealed that P had increased in R1 and R2
 367 and mostly decreased in R3–7 (Fig. 3). Along with the increase in annual P in the northern R1
 368 and R2 regions, a significant decline of ET_{stress} was observed in the same regions at such time
 369 scales. However, despite a decrease of P in R3–7, ET_{stress} also tended to decrease in large
 370 portions of these regions, except the Central Highlands (R5) and small areas of R3 and R4 and
 371 R7, where ET_{stress} increased. At inter-seasonal time scales, P in the northern R1 and R2 regions
 372 mostly increased during winter and fall and decreased during spring. While P in region R3
 373 primarily declined from winter to summer and only increased slightly in the fall over a majority
 374 of the region, P in regions R4–7 likewise increased only during wintertime (early periods of
 375 dry season) and tended to decrease during rest of the year. R1 was associated with a significant
 376 decrease in ET_{stress} from fall to spring and an insignificant decrease during summer, whereas
 377 R2 showed a significant decline throughout the year. ET_{stress} in R3–7 showed a decrease over
 378 the majority of the area year-round, except for a central portion of R4 and a western portion of
 379 R5, where ET_{stress} was likely to increase during the late dry and early rainy seasons (a seasonal
 380 change period). The Mekong River Delta in R7 and southeast region R6 experienced an
 381 increase in ET_{stress} during the spring and summer, respectively. Overall, P in northern R1–3
 382 regions primarily increased during winter and fall and decreased during spring, and P in
 383 southern R4–7 regions tended to increase during the early months of the dry season and
 384 primarily decreased in the rest of year. ET_{stress} showed a notable decrease in the northern R1
 385 and R2 regions as well as a majority of other regions year-round, except for a central portion
 386 of R4 and a western area in R5 with an increase during seasonal change period.

387 As can be seen in Fig. 4, the inter-annual increase rate for P was highest in R1 and R2 (> 10
 388 mm year^{-1}), which was consistent with a report by Le et al. (2020). The inter-seasonal
 389 investigation in this study revealed that the highest increase rate of these regions only occurs
 390 during fall seasons, and these regions even experienced a slight decrease in P ($< 5 \text{ mm season}^{-1}$)
 391 during spring. In other R3–7, the inter-annual decrease amounts of P were the largest (> 20
 392 mm year^{-1}) in the South Central Coastal (R4), Highland (R5) and Mekong River Delta (R5),
 393 which was in close agreement with Le et al. (2020). However, P in these regions increased ($>$
 394 5 mm season^{-1}) during winter and decreased during the rest of the one-year course. When it
 395 comes to ET_{stress} , a large decrease ($> 2 \text{ mm year}^{-1}$) over time was seen over a majority of the
 396 country. The northern R2 region experienced a large decline in magnitude at the inter-annual
 397 ($> 2 \text{ mm year}^{-1}$) and inter-seasonal ($> 1.5 \text{ mm season}^{-1}$) timescales, which can be attributed to
 398 the effect of an increase in P during the same period (Fig. 3 and 4) as well as a reduction in air
 399 temperatures (Le et al., 2020). Likewise, the inter-annual growth ($> 2 \text{ mm year}^{-1}$) of ET_{stress}
 400 was the highest in the Central Highlands (R5), which experienced the highest escalation of air
 401 temperatures in the country (Le et al., 2020). Our inter-seasonal comparison found that this
 402 large increase in ET_{stress} primarily occurred during the late dry and early rainy seasons. Again,
 403 these results indicate that ET_{stress} in Vietnam is sensitive to air temperature, particularly during
 404 rapid increases in temperatures over the southern regions (Le et al., 2020). These results also
 405 support the essential value of using ET-based rather than P-based indicators to quantify drought
 406 in Vietnam.

407

408 5.2. Performances of SESR in Vietnam

409 As the SESR is the key variable in the drought analysis used in this study, this section
410 thoroughly evaluates the performance of monthly SESR based on the SPEI in quantifying
411 drought conditions over the region of interest. R (a correlation coefficient) was used to make
412 inter-comparisons of these two indexes via a spatial map and boxplots (Fig. 5). Also, monthly
413 time series between these two drought indexes were constructed over seven sub-regions (Fig.
414 6) to describe their temporal variations during study period.

415 Correlations between the SESR and SPEI clearly varied among sub-regions. These two
416 indices were most closely correlated in the southeast (R6) and Mekong River Delta (R7), with
417 mean R values reaching 0.79 and 0.82, respectively (Fig. 5). Lower but consistent correlations
418 were observed in the north (R1 and R2) and Central Highlands (R5), with average R values of
419 approximately 0.58, 0.52, and 0.59, respectively. While the weakest correlation between these
420 two indices was found in sub-regions R3 and R4, with a mean value for R of approximately
421 0.22 and 0.41, respectively, and R frequently dropping below 0 (Fig. 5b), particularly in R3.
422 However, the SESR and SPEI generally followed a similar pattern in temporal variations
423 during study periods, which also agrees closely with the historical record (pink shades in Fig.
424 6) of Vietnam droughts. For example, both the SESR and SPEI effectively captured the
425 historical drought events in R4 and R5 in 2003 (Stojanovic et al., 2017), in R7 in 2019–2020
426 (Ty et al., 2022) and over the entire country in 2004–2005, 2010, and 2014–2016 (Stojanovic
427 et al., 2017; Le et al., 2020; Ty et al., 2022). However, the SPEI frequently showed less extreme
428 drought severity than did the SESR, including the drought events taking place in 2004–2005
429 across the country. In regions R3 and R4, the SPEI also regularly predicted the beginning and
430 ending of drought events sooner than those predicted by the SESR. Overall, the SESR
431 efficiently captured historical drought events during study periods, proving its usefulness in
432 depicting drought conditions in Vietnam. Also, the SESR was strongly and positively
433 correlated with SPEI over a majority of regions, except R3 and R4, where the two indexes
434 mainly presented negative correlations and inconsistencies in quantifying drought
435 characteristics.

436 By definitions, the SPEI and SESR track drought events that rely on a deficit between P
437 and PET (Beguería et al., 2014) and the ratio between AET and PET (Christian et al., 2019),
438 respectively. A drought event detected by the SPEI technically begins and ends at the same
439 time with a shortage P period, while droughts quantified by SESR have starting and ending
440 phases identical to those of periods with high ET_{stress} . Incorporating the results described in
441 Section 5.1.1, it is clear that regions R5–7 regularly experience large ET_{stress} during the dry
442 season, with extremely low P (Fig. 2). Likewise, regions R1 and R2 annually experience a
443 small amount of ET_{stress} , in which greater ET_{stress} primarily takes place during the dry winter
444 and spring. The two indices capture a similar period of drought and correlate closely with each
445 other over these regions. By contrast, ET_{stress} in R3 remains low during the dry winter but higher
446 during spring and summer, with increasing P magnitudes (Fig. 2). Drought events captured by
447 the SPEI in such regions therefore tend to start from a dry winter while those by the SESR are
448 likely to begin later, when ET_{stress} begins to intensify. Similarly, ET_{stress} in R4 inherently
449 remains high during the dry season and changes insignificantly when the rainy season begins
450 (Fig. 2); drought events captured by the SPEI in this region potentially end when P begins
451 escalating while those captured by the SESR last longer.

452 Not surprisingly, the SPEI is more accurate than the other P-based drought indices (i.e.,
453 Palmer drought index and Standardized Precipitation index) (Beguería et al., 2014), but it is
454 less efficient than the evapotranspiration-based drought index in monitoring agricultural
455 drought due to a lack of AET in its computations (Beguería et al., 2014; Pei et al., 2018).

456 Including PET in SPEI calculations only reflects the warming effects on drought (Pei et al,
457 2018) but does not account for the actual moisture status of the soil and vegetation during
458 extreme weather, which might be both reflected by AET and directly associated with
459 agricultural drought (Vicente-Serrano et al., 2010). Furthermore, AET varies across different
460 crops, and P has higher error than other variables (Kim and Rhee, 2016; Nguyen et al, 2023),
461 so using SPEI to identify agricultural drought might retain some uncertainties. It is worth noting
462 that this study does not refute the effectiveness of the SPEI in quantifying agricultural drought
463 (as evidence of positive results showed in most regions, except R3-4). However, integrating
464 the findings of this study with these in previously published reports lend us confidence that
465 SESR, which incorporates AET in its calculations, is more suitable to capture agricultural
466 drought condition under complex climate in several sub-regions of Vietnam. On the other hand,
467 it is widely acknowledged that the SPEI is superior to other drought indexes in quantifying
468 hydrological and ecological droughts in diverse of managed and natural systems (Beguería et
469 al., 2014). Accordingly, R3 and R4 might suffer from longer drought durations in the form of
470 transitions from hydrological and ecological droughts (reflected by the SPEI) to agricultural
471 droughts (captured by the SESR) that potentially evolve during the rainy months. In agreement
472 with Otkin et al. (2018), more than one type of drought can take place in a specific region in
473 the same period, and possibly convert from one type of drought to another as its impacts and
474 severities evolve. Generally, the SESR is able to capture the agricultural droughts in Vietnam
475 and has the potential to detect agricultural flash drought events over the country. We suggest
476 that future studies should apply multiple-indices to capture comprehensively characterizations
477 of droughts over Vietnam.

478

479 **5.3. Flash drought occurrence in Vietnam**

480 Flash drought occurrence across Vietnam was detected using the SESR and incorporating
481 multiple criteria related to rapid intensification and severity of drought as described in the
482 methodology sections. Fig. 7 and Fig. 8 depict the spatial identification, characteristics, and
483 drivers of flash drought over the study regions.

484 The results show that Vietnam has been suffering flash drought events, in which regions
485 R1–3 only has a low f_D of flash drought, with an annual mean below 3% per year and fewer
486 than 9 events during the study period (Fig. 7a and Fig. 8a). Regions R4–7 mostly experienced
487 a much higher f_D of flash drought, with an annual mean of up to 10% per year and more than 9
488 events during the study period. The annual mean f_D of flash drought could exceed 12% per
489 year, with 15–21 events during study period in the central area of R5, the southeast of R4, and
490 the majority of R6 and R7. A report by Christian et al. (2021) previously revealed that, in
491 comparison with global hotspots (i.e., Brazil and India), the tropical Indochinese Peninsula of
492 southeast Asia has experienced lesser but notable flash droughts. Regionally, the Lower
493 Mekong River basin area in Cambodia and a portion of Vietnam (the central area of R5 and
494 R7) regularly sees a higher frequency of flash drought events, compared with other areas in the
495 basin (Kang et al., 2022). Additionally, ET_{stress} in the northern regions R1–3 is dramatically
496 lower than in the southern regions R4–7 year-round due to different temperature and rainfall
497 regimes, as discussed in Section 5.1.1, providing evidence for a higher f_D of flash drought in
498 the southern R4–7 regions.

499 Otkin et al. (2018) underlined the need for multiple pathways of research to understand
500 regional drivers and characteristics of flash drought. Our study further found that flash droughts
501 in the northern and southern regions of Vietnam exhibited distinguishable drought

502 characteristics (Fig. 7b). Flash droughts tended to occur during the dry winter (December to
503 February) in R1 and during hot summers (May to July) in R2 and R3 with small PDA
504 magnitudes (below 20% of each region's area. In the southern regions of R4–7, flash droughts
505 frequently appeared during the dry season (December to April), and R7 in particular
506 experienced a high f_D of flash droughts during the rainy season (July to August). Flash droughts
507 predominantly occurred in less than 20% of R4's area, while it reached 30% of regions R5–7,
508 particularly region R5 and R6, where flash drought sometimes covered more than 50% of the
509 region. Most of sub-regions showed a decrease in PDA, most notably R5 and R6, which saw a
510 statistically significant decline in PDA over the study period (Fig. 7b). From a climatological
511 standpoint, changes in the occurrence and spatial extent of flash drought are a function of
512 ET_{stress} according to variations in PET and AET. Specifically, an increase in PET can be
513 associated with a rise in vapor pressure deficit and temperature, which are critical factors in
514 climate change (Hobbins and Wood, 2012). One common feature over seven sub-regions is
515 that of a high f_D of flash drought arising during times of high ET_{stress} , as discussed in Section
516 5.1.1. For example, in one year, R7 experienced a second period (July and August) with a
517 relatively large f_D of flash drought, which can be attributed to the effects of a second
518 intensification of ET_{stress} (Fig. 2). Likewise, the decline in PDA across most sub-regions was
519 due to a decrease in ET_{stress} over the majority of Vietnam, as detailed in Section 5.1.2. It is
520 worth clarifying that, despite the increase over time in ET_{stress} in regions R5 and R7, a reduction
521 in PDA persisted over those areas. This can be mainly attributed to the fact that the ET_{stress} in
522 these regions primarily escalated during the late dry season (March to May), whereas flash
523 drought took place primarily during the early dry season (December to March), when such
524 regions experienced reduced ET_{stress} (Fig. 3 and Fig. 4). Moreover, a change in the spatial
525 coverage of a flash drought may be driven by a teleconnection phase (i.e., ENSO) (Christian et
526 al., 2021). Consequently, decreases in PDA over most regions are possibly due to the weakness
527 of El Niño events over the past two decades (Hu and Fedorov, 2018). The linkage between
528 Vietnam flash droughts and ENSO climate modes is discussed in more detail in Section 5.4.

529 Next, to examine the drivers of flash droughts over the region of interest, standardized air
530 temperature and PET anomalies at three ground stations in areas with large numbers of flash
531 drought events were examined (Fig. 8b). The time series typically indicated that a flash drought
532 event (light yellow) took place during periods when the SESR rapidly and significantly
533 decreased (most often dropping below -1) while anomalous air temperature and PET increased
534 by more than 1 (Fig. 8b). This phenomenon was most evident during these selected flash
535 drought events due to their rapid intensification over a relatively long period. Additionally, as
536 noted in Section 5.1.1 and 5.1.2, ET_{stress} conditions over Vietnam are insignificantly sensitive
537 to P, and flash drought in the country can be categorized as 'heat wave' flash droughts due to
538 their simultaneous manifestation during periods of elevated air temperatures and PET
539 anomalies (Otkin et al., 2018). This type of flash drought can have profound impacts on
540 vegetated areas (Otkin et al., 2018; Wang et al., 2016), suggesting an avenue for future research
541 focusing on the impacts of flash drought on vegetation and crops in Vietnam. Overall, our study
542 confirms that Vietnam has experienced flash drought events, particularly in the central
543 highlands (R5), southeast (R6), and Mekong Delta River (R7), with approximately 12–21
544 events recorded over the last two decades, primarily in the dry season (December to April).
545 Flash drought development in Vietnam is controlled by heat waves due to higher-than-normal
546 air temperatures and PET. We therefore encourage more research on the interactions between
547 heat wave flash droughts and agricultural impacts in Vietnam.

548

549 5.4. Impacts of ENSO on flash droughts in Vietnam

550 Identifying the teleconnection of ENSO with regional hydrology could bolster
 551 hydrological management efforts (Abteu and Trimble, 2010), we thus discuss the linkage
 552 between flash drought and ENSO phase in this section. Initially, the correlation between the
 553 monthly mean SESR and monthly ENSO indices is represented by a spatial distribution of R
 554 values in Vietnam (Fig. 9). Signs of ONI, Niño 3.4, and MEI were inverted to consistently
 555 indicate El Niño and La Niña events in the same manner as other indices, such that negative
 556 values of ENSO indices now represent El Niño and vice versa. This section also investigates
 557 patterns of yearly frequencies of flash droughts in the southern R4–7 regions, which have the
 558 highest f_D rates in the country, along with ENSO events, as shown by the ONI over study
 559 periods as the time series illustrates in Fig. 10.

560 Throughout the country, spatial maps indicate discrepancies in relationships between the
 561 SESR and ENSO indices among sub-regions (Fig. 9). In northern regions, the association
 562 between the SESR and the five ENSO indices is generally weak (with most R values below
 563 0.2) in R1, R3 and the northern portion of R4, whereas R2 exhibited a slightly higher
 564 association (R values within a range of 0.2–0.3) with ONI, Niño 3.4, and MEI indices. Unlike
 565 the northern regions, the SESR showed a markedly stronger correlation (R varies within a range
 566 of 0.3–0.6), with all five ENSO indices for the southern regions (R5–7 and the southeast area
 567 of R4), and a particularly large correlation evident between the SESR and TNI (most R values
 568 above 0.5). More precisely, time series analysis of ENSO events and flash drought occurrence
 569 in R4-7 further revealed a similar pattern of flash drought occurrence and ENSO climate mode
 570 (Fig. 10). Years characterized by La Niña events (2006, 2008–2009, 2011–2012, and 2017–
 571 2018) were associated with a low f_D of flash drought (mostly below or around 10% per year),
 572 whereas those featuring El Niño events (2003, 2005, 2007, 2010, 2016–2017, and 2019) were
 573 involved in a significantly higher f_D of flash drought, ranging from 12% to 20% per year.
 574 Surprisingly, years with neutral conditions (2004, 2013–2014, and 2020) showed a
 575 considerable f_D of flash drought of approximately 15% per year, particularly in 2004, when the
 576 flash drought occurrence rate in R6 approached nearly 30%. Generally, flash droughts in
 577 Vietnam are influenced by the ENSO climate mode, with a significant correlation identified in
 578 southern regions (R4–7) and a less pronounced connection in the north (R1–3).

579 Historically, during years with El Niño events, prolonged drought events would commonly
 580 occur over all of Vietnam (Le et al., 2020, 2019). Statistically, Christian et al. (2021) found
 581 that the Indochinese Peninsula was one of a few regions in the world (along with southwest
 582 Africa and northwest North America) to show a significant association between flash drought
 583 events and ENSO climate modes. It is therefore not surprising that the ENSO phase also had
 584 impacts on flash drought events in Vietnam. Among sub-regions, the contrasting association
 585 between ENSO events and flash droughts in the northern and southern regions was likely the
 586 result of the diverse rainfall regimes and temperature conditions over these areas. While rainfall
 587 and temperature in Northern R1-3 are mainly dominated by the East Asian summer monsoon
 588 system (Buckly et al., 2014), those in the southern R4–7 regions are driven by the southeast
 589 Asian summer monsoon climate (Yan et al., 2018). Compared with the East Asian monsoon,
 590 the Southeast Asian summer monsoon is closer to the equator, where the warmest sea-surface
 591 temperature has been reported, along with the strongest example of coupling between ocean
 592 and atmospheric circulation. Moreover, peak ENSO events regularly take place from October
 593 to March, coinciding with a cool fall and cold winter in northern regions (Section 5.1.1), when
 594 flash droughts occur infrequently (Section 5.3). Any direct link between ENSO and flash
 595 drought in these regions is unclear but cannot be ruled out, as evidence of a correlation between

596 the SESR and ENSO indices was found in this study. In contrast, peak ENSO times coincided
597 with the dry season of southern regions in Vietnam (December to April) (Section 5.1.1), when
598 flash droughts occur most frequently in such regions (Hu and Fedorov, 2018), suggesting a
599 stronger susceptibility of flash droughts to ENSO effects in the south than in the north of
600 Vietnam.

601 Delving deeper into the influences of ENSO on flash drought in Southern Vietnam, this
602 study found that the frequency of flash drought occurrence rose in El Niño years while low
603 frequencies were associated with La Niña years. The El Niño phase typically reinforces the
604 hotter- and drier-than-normal conditions over southeast Asia (Juneng and Tangang, 2005), as
605 evaporative demand in the atmosphere rises, resulting in drought events. Under such a weather
606 context, the rapid intensification of evaporative stress could lead to the onset of flash drought.
607 Conversely, La Niña years are accompanied by wetter- and cooler-than-normal conditions that
608 reduce the likelihood of flash droughts (Christian et al., 2021). By those definitions, neutral
609 years inherently have a greater possibility of complex dry and hot events than do La Niña years,
610 particularly during neutral years that is followed by an El Niño year with much hotter and drier
611 conditions (Feng and Hao, 2021). For example, 2004 was an ENSO-neutral year sandwiched
612 between two El Niño years (2003 and 2005), which apparently experienced a prolonged dry
613 and hot extreme, followed by a high frequency of flash drought occurrence. Overall, flash
614 drought occurrence in Vietnam is closely related to ENSO events, with a notable emphasis in
615 southern regions, where flash drought can be promoted during either El Niño or neutral
616 conditions.

617

618 6. Conclusions

619 This paper aimed to investigate the occurrence and characteristics of flash droughts in
620 Vietnam, along with its driving factors such as rainfall, evaporative stress, and ENSO phases.
621 It focused on: (1) tracking flash drought occurrence and its characteristics in Vietnam using the
622 SESR and flash drought criteria, and (2) examining the impacts of ENSO phase on flash
623 drought occurrence in Vietnam.

624 In term of quantifying drought conditions, monthly SESR values effectively presented
625 historical drought events over the study period and closely matched the SPEI over most study
626 regions, with the exception of the Central Coast (R3 and R4). As Vietnam potentially
627 undergoes more than one drought type on the same periods, using a single drought index
628 therefore cannot adequately reflect the features and duration of drought in Vietnam, particularly
629 in areas with complicated climate conditions (i.e., the central coastal region, R3 and R4).

630 By incorporating four strict criteria that fully describe the characteristics of a flash drought
631 event into pentad SESR calculations and their Δ SESR, this study successfully detected flash
632 drought occurrence over Vietnam. Over the last two decades, regions R1–3 and the majority
633 of R4 endured fewer than 9 flash drought events, most covering less than 20% of drought area,
634 while the remaining areas (R5–7 and the southeast area of R4) underwent between 12 and 21
635 events covering from 30% to over 50% of each region's area. Characteristically, flash drought
636 events primarily occurred during dry winters in the northern R1 region, during hot summers in
637 northern regions R2 and R3, and during the dry season in southern regions R4–7, most notably
638 when anomalous PET and temperatures were positive and exacerbating. We also found that the
639 ENSO climate mode affected flash drought occurrence in Vietnam, with a notable association
640 in the southern R5–7 regions, where a high flash drought frequency can appear in either El

641 Niño or neutral conditions. During La Niña years, the occurrence of flash drought is less likely
 642 but still possible, highlighting the need for ongoing preparedness and readily available impact
 643 mitigation strategies. Overall, our study once again confirmed the occurrence of flash drought
 644 extreme events over Vietnam, particularly in southern regions of the country. These bridges a
 645 research gap in our understanding of the characteristics and drivers of drought occurrences in
 646 Vietnam, which gives an idea of where our findings fall among existing Vietnam drought
 647 publications. We encourage more research to better understand the impacts of flash droughts
 648 on agriculture and other aspects of Vietnam as well as other agriculture-oriented countries.

649

650 Acknowledgments

651 This research was supported by a grant (2021-MOIS35-003) of 'Policy-linked Technology
 652 Development Program on Natural Disaster Prevention and Mitigation' funded by Ministry of
 653 Interior and Safety (MOIS, Korea). This research was supported by the BK21 FOUR (Fostering
 654 Outstanding Universities for Research) funded by the Ministry of Education (MOE, Korea)
 655 and National Research Foundation of Korea (NRF). The authors are grateful to the developers,
 656 managers, and funding organizations for freely providing GLEAM evapotranspiration data,
 657 IMERG rainfall products, and ENSO climate indices.

658

659 References

- 660 [Abteu, W., Trimble, P., 2010. El Niño-Southern Oscillation Link to South Florida Hydrology
 661 and Water Management Applications. *Water Resour. Manag.* 24, 4255–4271.
 662 <https://doi.org/10.1007/s11269-010-9656-2>](#)
- 663 [Aghakouchak, A., Cheng, L., Mazdiyasni, O., A.F., 2014. Global warming and changes in risk
 664 of concurrent climate extremes: Insights from the 2014 California drought. *Geophys. Res.
 665 Lett.* <https://doi.org/10.1002/2014GL062308>](#)
- 666 [Beck, H.E., Zimmermann, N.E., McVicar, T.R., Vergopolan, N., Berg, A., Wood, E.F., 2018.
 667 Present and future Köppen-Geiger climate classification maps at 1-km resolution.
 668 *Scientific data*, 5, 180214. <https://doi.org/10.1038/s41597-020-00616-w>](#)
- 669 [Beguería, S., Vicente-Serrano, S.M., Reig, F., Latorre B., 2014. Standardized precipitation
 670 evapotranspiration index \(SPEI\) revisited: parameter fitting, evapotranspiration models,
 671 tools, datasets and drought monitoring. *Int. J. Climatol.* 34, 3001-3023.
 672 <https://doi.org/10.1002/joc.3887>](#)
- 673 [Buckly, B. M., Fletcher, R., Wang, S.S., Zottoli, B., Pottier, C., 2014. Monsoon extremes and
 674 society over the past millennium on mainland Southeast Asia. *Quat. Sci. Rev. J.* 1–19.
 675 <http://dx.doi.org/10.1016/j.quascirev.2014.04.022>](#)
- 676 [Christian, J.I., Basara, J.B., Hunt, E.D., Otkin, J.A., Mishra, V., Xiao, X., Randall, R.M.,
 677 Furtado, J.C., 2021. Global distribution, trends, and drivers of flash drought occurrence.
 678 *Nat. communications* 1–11. <https://doi.org/https://doi.org/10.1038/s41467-021-26692-z>](#)
- 679 [Christian, J.I., Basara, J.B., Otkin, J.A., Hunt, E.D., Wakefield, R.A., Flanagan, P.X., Xiao, X.,
 680 2019. A methodology for flash drought identification: Application of flash drought](#)

- 681 frequency across the United States. *J. Hydrometeorol.* 20, 833–846.
682 <https://doi.org/10.1175/JHM-D-18-0198.1>
- 683 Dai, A., 2012. Increasing drought under global warming in observations and models. *Nat. Clim.*
684 *Chang.* 1–15. <https://doi.org/10.1038/NCLIMATE1633>
- 685 Donohue, R.J., McVicar, T.R., Roderick, M.L., 2010. Assessing the ability of potential
686 evaporation formulations to capture the dynamics in evaporative demand within a
687 changing climate. *J. Hydrol.* 386, 186–197. <https://doi.org/10.1016/j.jhydrol.2010.03.020>
- 688 Forda, T.W., Labosier, C.F., 2017. Meteorological conditions associated with the onset of flash
689 drought in the Eastern United States. *Agric. For. Meteorol.* 414–423.
690 <https://doi.org/http://dx.doi.org/10.1016/j.agrformet.2017.08.031>
- 691 Feng, S., Hao, Z., 2021. Quantitative contribution of ENSO to precipitation-temperature
692 dependence and associated compound dry and hot events. *Atmos. Res.* 260, 105695.
693 <https://doi.org/10.1016/j.atmosres.2021.105695>
- 694 Gocic, M., Trajkovic, S., 2013. Analysis of changes in meteorological variables using Mann-
695 Kendall and Sen’s slope estimator statistical tests in Serbia. *Glob. Planet. Change* 100,
696 172–182. <http://dx.doi.org/10.1016/j.gloplacha.2012.10.014>
- 697 Godfray, H.C.J., Beddington, J.R., Crute, I.R., Haddad, L., Lawrence, D., Muir, J.F., Pretty, J.,
698 Robinson, S., Thomas, S.M., Toulmin, C., 2010. Food Security: The Challenge of Feeding
699 9 Billion People. *Science* 327:812–818. *Science* (80-.).
- 700 Hamed, K.H., 2009. Exact distribution of the Mann-Kendall trend test statistic for persistent
701 data. *J. Hydrol.* <https://doi.org/10.1016/j.jhydrol.2008.11.024>
- 702 Hamed, K.H., Rao, A.R., 1998. A modified Mann-Kendall trend test for autocorrelated data. *J.*
703 *Hydrol.* 204, 182–196. <https://doi.org/10.1016/j.atmosres.2018.06.019>
- 704 Hobbins, M., Wood, A., 2012. What Drives the Variability of Evaporative Demand across the
705 Conterminous United States? *J. Hydrometeorol.* [http://dx.doi.org/10.1016/10.1175/JHM-](http://dx.doi.org/10.1016/10.1175/JHM-D-11-0101.1)
706 [D-11-0101.1](http://dx.doi.org/10.1016/10.1175/JHM-D-11-0101.1)
- 707 Hobbins, M.T., Wood, A., McEvoy, D.J., Huntington, J.L., Morton, C., Anderson, M., Hain,
708 C., 2016. The evaporative demand drought index. Part I: Linking drought evolution to
709 variations in evaporative demand. *J. Hydrometeorol.* 17, 1745–1761.
710 <https://doi.org/10.1175/JHM-D-15-0121.1>
- 711 Hu, S., Fedorov, A. V., 2018. Cross-equatorial winds control El Niño diversity and change.
712 *Nat. Clim. Chang.* 8, 798–802. <https://doi.org/10.1038/s41558-018-0248-0>
- 713 Hu, X., Ren, H., Tansey, K., Zheng, Y., Ghent, D., Liu, X., Yan, L., 2019. Agricultural drought
714 monitoring using European Space Agency Sentinel 3A land surface temperature and
715 normalized difference vegetation index imageries. *Agric. For. Meteorol.* 279, 107707.
716 <https://doi.org/10.1016/j.agrformet.2019.107707>
- 717 Huffman, G.J., 2018. NASA Global Precipitation Measurement (GPM) Integrated Multi-
718 satellitE Retrievals for GPM (IMERG).

- 719 Huffman, G.J., Bolvin, D.T., Nelkin, E.J., Tan, J., 2020. Integrated Multi-satellite Retrievals
720 for GPM (IMERG) Technical Documentation, American Journal of Orthodontics and
721 Dentofacial Orthopedics. <https://doi.org/10.1016/j.ajodo.2020.07.011>
- 722 Juneng, L., Tangang, F.T., 2005. Evolution of ENSO-related rainfall anomalies in Southeast
723 Asia region and its relationship with atmosphere - Ocean variations in Indo-Pacific sector.
724 *Clim. Dyn.* <https://doi.org/10.1007/s00382-005-0031-6>
- 725 Kang, H., Sridhar, V., Ali, S.A., 2022. Climate change impacts on conventional and flash
726 droughts in the Mekong River Basin. *Sci. Total Environ.* 838, 155845.
727 <http://dx.doi.org/10.1016/j.scitotenv.2022.155845>
- 728 Kim, D., Rhee, J., 2016. A drought index based on actual evapotranspiration from the Bouchet
729 hypothesis. *Geophys. Res. Lett.* 43, 10,277-10,285.
730 <https://doi.org/10.1002/2016GL070302>
- 731 Kiladis, G. N., and H. van Loon, 1988: The Southern Oscillation. Part VII: Meteorological
732 anomalies over the Indian and Pacific sectors associated with the extremes of the
733 oscillation. *Mon. Wea. Rev.*, 116, 120-136.
- 734 Le, M.H., Kim, H., Moon, H., Zhang, R., Lakshmi, V., Nguyen, L.B., 2020. Assessment of
735 drought conditions over Vietnam using standardized precipitation evapotranspiration
736 index, MERRA-2 re-analysis, and dynamic land cover. *J. Hydrol. Reg. Stud.* 32, 100767.
737 <https://doi.org/10.1016/j.ejrh.2020.100767>
- 738 Le, P.V.V., Phan-Van, T., Mai, K. V., Tran, D.Q., 2019. Space-time variability of drought over
739 Vietnam. *Int. J. Climatol.* 39, 5437–5451. <https://doi.org/10.1002/joc.6164>
- 740 Li, J., Wang, Z., Wu, X., Chen, J., Guo, S., Zhang, Z., 2020. A new framework for tracking
741 flash drought events in space and time. *Catena* 194, 104763.
742 <https://doi.org/10.1016/j.catena.2020.104763>
- 743 Lyon, B., 2004. The strength of El Niño and the spatial extent of tropical drought Bradfield.
744 *Geophys. Res. Lett.* 31, L21204. <https://doi.org/10.1029/2004GL020901>
- 745 Miralles, D.G., Holmes, T.R.H., De Jeu, R.A.M., Gash, J.H., Meesters, A.G.C.A., Dolman,
746 A.J., 2011. Global land-surface evaporation estimated from satellite-based observations.
747 *Hydrol. Earth Syst. Sci.* 15, 453–469. <https://doi.org/10.5194/hess-15-453-2011>
- 748 Miralles, D.G., Jiménez, C., Jung, M., Michel, D., Ershadi, A., McCabe, M.F., Hirschi, M.,
749 Martens, B., Dolman, A.J., Fisher, J.B., Mu, Q., Seneviratne, S.I., Wood, E.F., Fernández-
750 Prieto, D., 2016. The WACMOS-ET project - Part 2: Evaluation of global terrestrial
751 evaporation data sets. *Hydrol. Earth Syst. Sci.* <https://doi.org/10.5194/hess-20-823-2016>
- 752 Narasimhan, B., Srinivasan, R., 2005. Development and evaluation of Soil Moisture Deficit
753 Index (SMDI) and Evapotranspiration Deficit Index (ETDI) for agricultural drought
754 monitoring. *Agric. For. Meteorol.* 133, 69–88.
755 <https://doi.org/10.1016/j.agrformet.2005.07.012>
- 756 Nguyen, D.Q., Renwick, J., McGregor, J., 2014. Variations of surface temperature and rainfall
757 in Vietnam from 1971 to 2010. *R. Meteorol. Soc.* 34, 249-264.
758 <https://doi.org/10.1002/joc.3684>

- 759 Nguyen, H., Shaw, R., 2011. Drought risk management in Vietnam. Chapter 8 Droughts in
760 Asian Monsoon Region. Emerald Group Publishing Limited, Bingley, UK, pp. 141–
761 161. [https://doi.org/10.1108/S2040-7262\(2011\)0000008014](https://doi.org/10.1108/S2040-7262(2011)0000008014)
- 762 Nguyen, M.N., Choi, M., 2022. Advances in evapotranspiration prediction using gross primary
763 productivity based on eco-physiological constraints. *Hydrol. Process.* 36, 1–19.
764 <https://doi.org/10.1002/hyp.14628>
- 765 Nguyen, N.M., Choi, M., 2023. Evapotranspiration partitioning and agricultural drought
766 quantification with an optical trapezoidal framework. *Agric. For. Meteorol.*, 338, 109520.
767 <https://doi.org/10.1016/j.agrformet.2023.109520>
- 768 Otkin, J.A., Anderson, M.C., Hain, C., Mladenova, I.E., Basara, J.B., Svoboda, M., 2013.
769 Examining rapid onset drought development using the thermal infrared-based evaporative
770 stress index. *J. Hydrometeorol.* 14, 1057–1074. <https://doi.org/10.1175/JHM-D-12-0144.1>
- 772 Otkin, J.A., Shafer, M., Svoboda, M., Wardlow, B., Anderson, C., Hain, C., Basara, J., 2015.
773 Facilitating the Use of Drought Early warning information through intertations with
774 Agricultural Stakeholders. *Am. Meteorol. Soc.* <https://doi.org/10.1175/BAMS-D-14-00219.1>
- 776 Otkin, J.A., Svoboda, M., Hunt, E.D., Ford, T.W., Anderson, M.C., Hain, C., Basara, J.B., 2018.
777 Flash droughts: A review and assessment of the challenges imposed by rapid-onset
778 droughts in the United States. *Bull. Am. Meteorol. Soc.* 99, 911–919.
779 <https://doi.org/10.1175/BAMS-D-17-0149.1>
- 780 Paul, G., Agrawal, N., Dollar, D., 2004. Economic Growth, Poverty, and Household Welfare
781 in Vietnam. World Bank regional and sectoral studies. ISBN 0-8213-5543-0
- 782 Sen, P.K., 1968. Estimates of the Regression Coefficient Based on Kendall's Tau. *J. Am. Stat.*
783 *Assoc.* 324, 1379-1389. <http://www.jstor.org/stable/2285891>
- 784 Smith, A.B., Katz, R.W., 2013. US billion-dollar weather and climate disasters: Data Sources ,
785 Trends , Accuracy and Biases. *Nat. Hazards*, 67, 387-410. <https://doi.org/10.1007/s11069-013-0566-5>
- 787 Stojanovic, M., Liberato, M.L.R., Sorí, R., Vázquez, M., Tan, P.V., Hieu, D.V., Cong, T.H.,
788 Nguyen, P.N.B., Nieto, R., Gimeno, L., 2020. Trends and Extremes of Drought Episodes
789 in Vietnam Sub-Regions during 1980–2017 at Different Timescales. *Water (Switzerland)*,
790 12, 813. <http://dx.doi.org/10.3390/w12030813>
- 791 Svoboda, M., LeComte, D., Hayes, M., Heim, R., Gleason, K., Angel, J., Rippey, B., Tinker,
792 R, Palecki, M., Stooksbury, D., Miskus, D., Stephens, S., 2002. The drought monitor. *Am.*
793 *Meteorol. Soc.* 1181-1190. <https://doi.org/10.1175/1520-0477-83.8.1181>
- 794 Thanh, H.V., Duc, T.N., Van, T.P., 2014. Evolution of meteorological drought characteristics
795 in Vietnam during the 1961–2007 period. *Theory Appl. Climatol.* 118, 367-375.
796 <http://dx.doi.org/10.1007/s00704-013-1073-z>
- 797 Tue, V.M., Raghavan, S.V., Minh, P.D., Shie-Yui, L., 2015. Investigating drought over the
798 Central Highland, Vietnam, using regional climate models. *J. Hydrol.* 526, 265–273.

- 799 <http://dx.doi.org/10.1016/j.jhydrol.2014.11.006>
- 800 Ty, T.V., Lavane, K., Nguyen, P.C., Downes, N.K., Nam, N.D.G., Minh, H.V.T., Kumar, P.,
801 2022. Assessment of Relationship between Climate Change, Drought, and Land Use and
802 Land Cover Changes in a Semi-Mountainous Area of the Vietnamese Mekong Delta. *Land*.
803 <https://doi.org/10.3390/land11122175>
- 804 Trenberth, K. E., Stepaniak, D. P., 2001. Indices of El Nino Evolution. *J. Climate*, 14, 1697-
805 1701.
- 806 Vicente-Serrano, S.M., 2010. A New Global 0.58 Gridded Dataset (1901–2006) of a
807 Multiscalar Drought Index: Comparison with Current Drought Index Datasets Based on
808 the Palmer Drought Severity Index S. J. Hydrometeorol.
809 <http://dx.doi.org/10.1175/2010JHM1224.1>
- 810 Pei, W., Fu, Q., Liu, D., Li, T., 2018. A drought index for Rainfed agriculture: The
811 Standardized Precipitation Crop Evapotranspiration Index (SPCEI). *Hydrol. Process.* 33,
812 803-815. <http://dx.doi.org/10.1002/hyp.13365>
- 813 Wang, L., Yuan, X., Xie, Z., Wu, P., Li, Y., 2016. Increasing flash droughts over China during
814 the recent global warming hiatus. *Sci. Rep.* 6, 1–8. <https://doi.org/10.1038/srep30571>
- 815 Wolter, K., and M.S. Timlin, 1993: Monitoring ENSO in COADS with a seasonally adjusted
816 principal component index. Proc. of the 17th Climate Diagnostics Workshop, Norman,
817 OK, NOAA/NMC/CAC, NSSL, Oklahoma Clim. Survey, CIMMS and the School of
818 Meteor., Univ. of Oklahoma, 52-57.
- 819 Wolter, K., and M. S. Timlin, 1998: Measuring the strength of ENSO events - how does
820 1997/98 rank? *Weather*, 53, 315-324. DOI: 10.1002/j.1477-8696.1998.tb06408.x.
- 821 Yan, X., Konopka, P., Ploeger, F., Tao, M., Muller, R., Michelle, L.S., Bian, J., Riese, M.,
822 2018. El Niño Southern Oscillation influence on the Asian summer monsoon anticyclone.
823 *Atmos. Chem. Phys.* 18, 8079–8096.
- 824 Yao, N., Li, Y., Lei, T., Peng, L., 2018. Drought evolution, severity and trends in mainland
825 China over 1961–2013. *Sci. Total Environ.* 616–617, 73–89.
826 <https://doi.org/10.1016/j.scitotenv.2017.10.327>
- 827 Yao, Y., Liang, S., Qin, Q., Wang, K., 2010. Monitoring drought over the conterminous United
828 States using MODIS and NCEP reanalysis-2 data. *J. Appl. Meteorol. Climatol.* 49, 1665–
829 1680. <https://doi.org/10.1175/2010JAMC2328.1>
- 830 Zaki, M.K., Noda, K., 2022. A Systematic Review of Drought Indices in Tropical Southeast
831 Asia. *Atmosphere (Basel)*. <https://doi.org/10.3390/atmos13050833>
- 832 Zhou, J., Wang, Y., Su, B., Wang, A., Tao, H., Zhai, J., Kundzewicz, Z. W., Jiang, T.,
833 2020. Choice of potential evapotranspiration formulas influences drought assessment: A
834 case study in China. 242, 104979. <https://doi.org/10.1016/j.atmosres.2020.104979>

835 **Abstract**

836 A flash drought is a recently defined extreme event that has destructive impacts on
837 agriculture as well as other elements of society and ecosystems. Understanding where and
838 when flash droughts occur can improve predictability and mitigation strategies for countries
839 with economies that rely on agriculture. This study represents the first investigation of flash
840 drought occurrences in Vietnam, one of the largest agricultural exporters in the world, using
841 the standardized evaporative stress ratio (SESR). Monthly SESR data captured historical
842 sustained drought events across the study period and exhibited a pattern similar to that shown
843 by the standardized precipitation evapotranspiration index over most of the study region, with
844 Pearson's correlations mostly ranging from 0.52 to 0.82. Results of the SESR analysis at a
845 pentad timescale indicate that flash droughts did occur in the country over the last two decades,
846 with the northern regions and a majority of the south-central coast experiencing fewer than 9
847 flash drought events that covered less than 20% of each region. The remaining southern areas
848 of the country were subjected to a much higher flash drought frequency, with 12 to 21
849 occurrences covering from 30% to more than 50% of the area in each region, typically during
850 the dry season and exacerbated by anomalies of potential evapotranspiration and temperature.
851 This research also revealed that flash droughts in Vietnam were correlated with the El Niño
852 Southern Oscillation climate phenomenon, particularly in the southern regions, where a high
853 flash drought frequency could take place under either El Niño or neutral conditions. This study
854 provides new evidence to support the development of a comprehensive overview of drought in
855 Vietnam, the country's drought mitigation strategies, and water management policies.

856

857

858 Author contribution:

859 **My Ngoc Nguyen:** Conceptualization, Methodology, Resources, Software, Formal analysis, Writing-
860 original Draft, Visualization.

861 **Minha Choi:** Supervision, Project administration, Funding acquisition, Writing-Review and Editing.

862

863

864 Declaration of interests

865

866 The authors declare that they have no known competing financial interests or personal
867 relationships that could have appeared to influence the work reported in this paper.

868

869 The authors declare the following financial interests/personal relationships which may be
870 considered as potential competing interests:

871



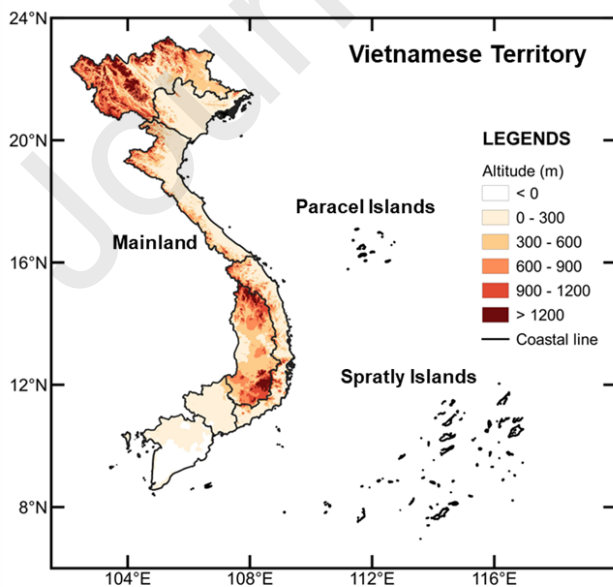
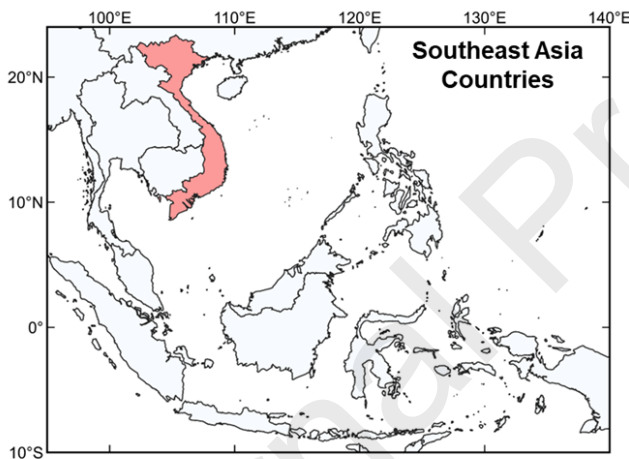
872

873

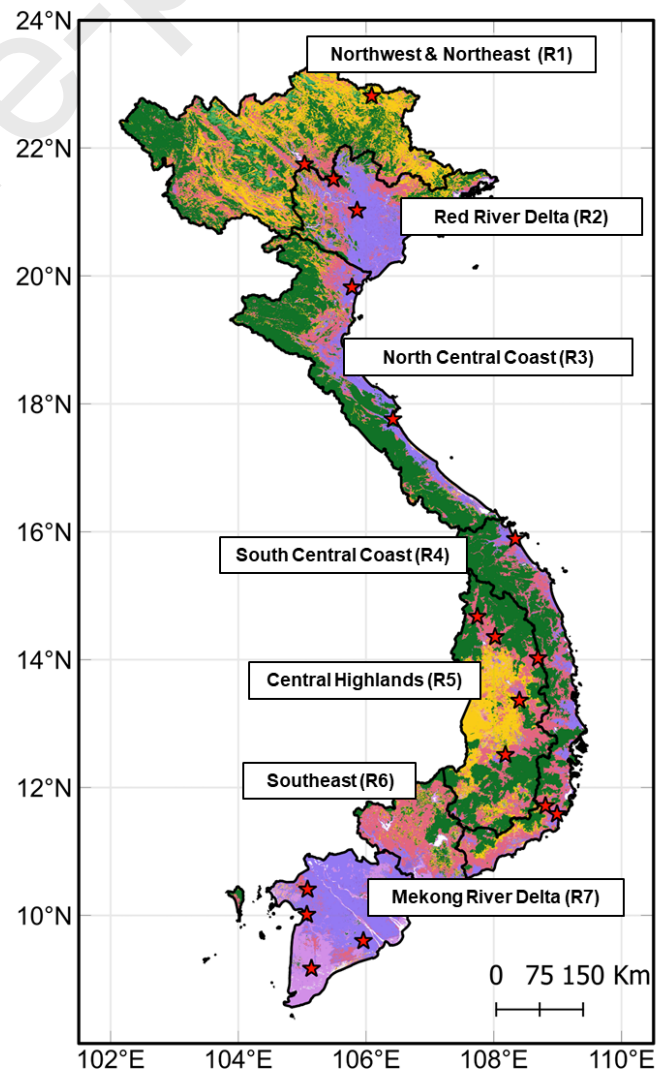
874

875

876



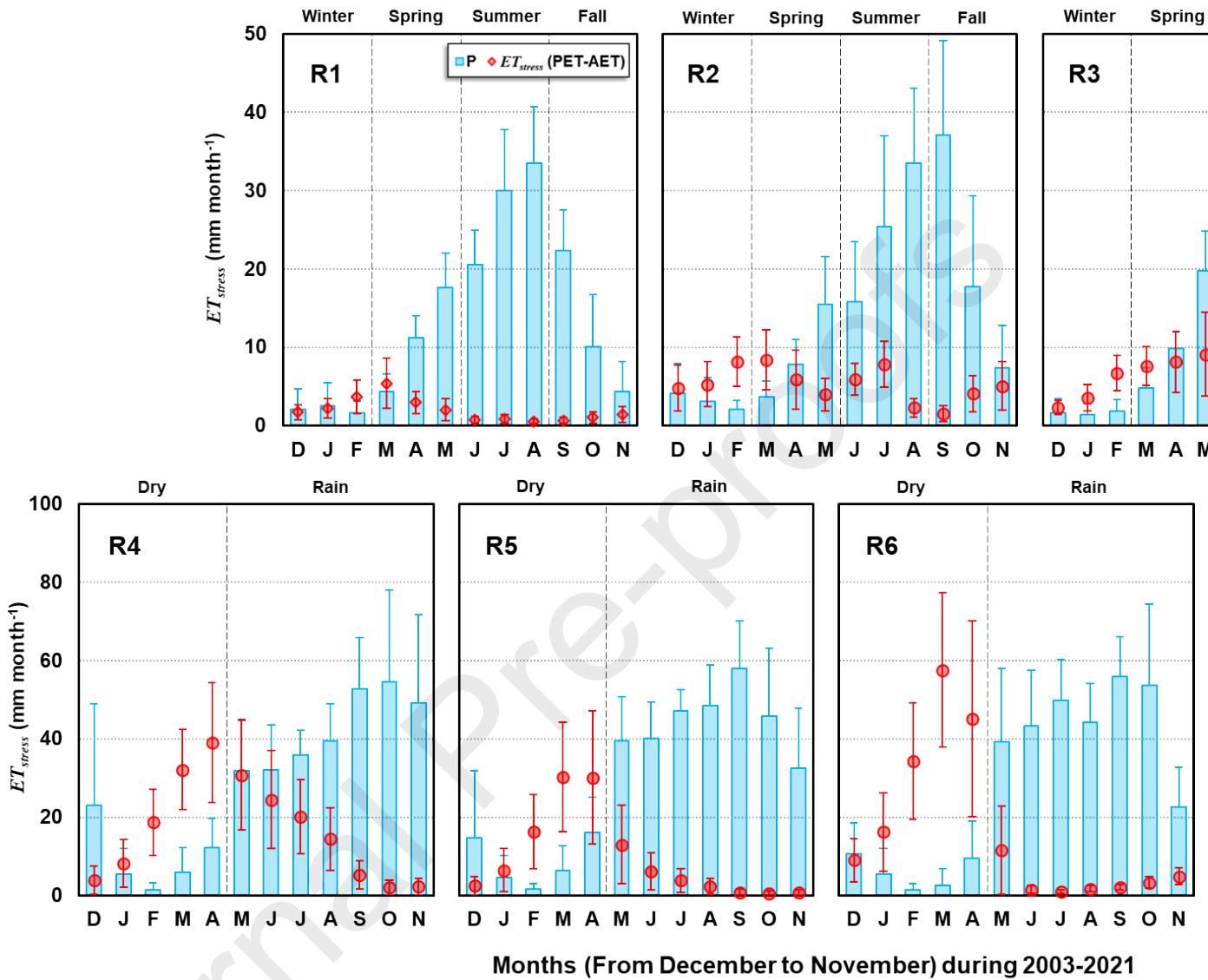
STUDY AREA

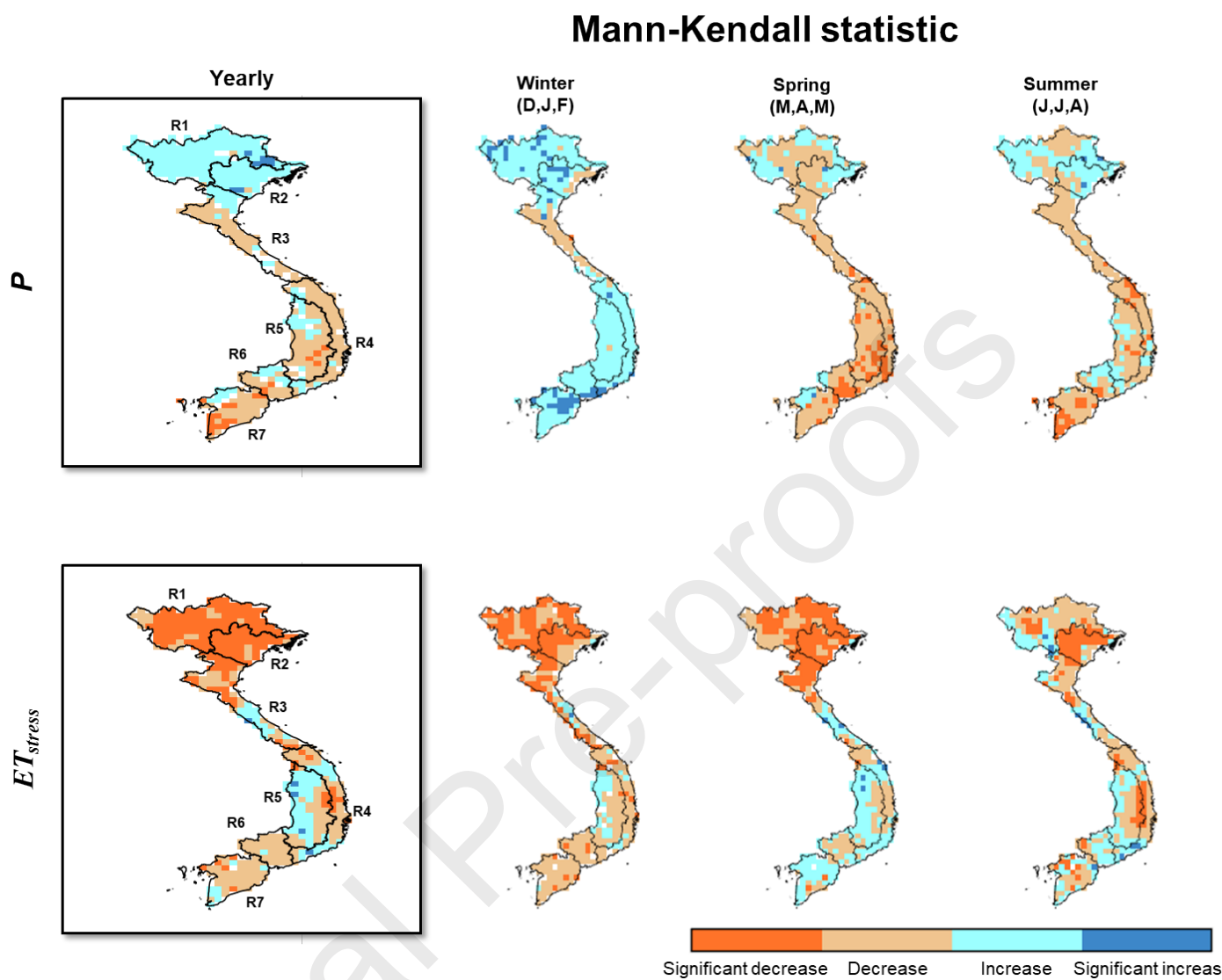


- Station ID
- TB
 - BG
 - QC
 - HN
 - BD
 - TH
 - TM
 - HA
 - PR
 - KT
 - DM
 - GS
 - AK
 - AP
 - TT
 - RG
 - ST
 - CM
- LE
- Green
 - Orange
 - Yellow
 - Purple
 - Red
 - Grey

877

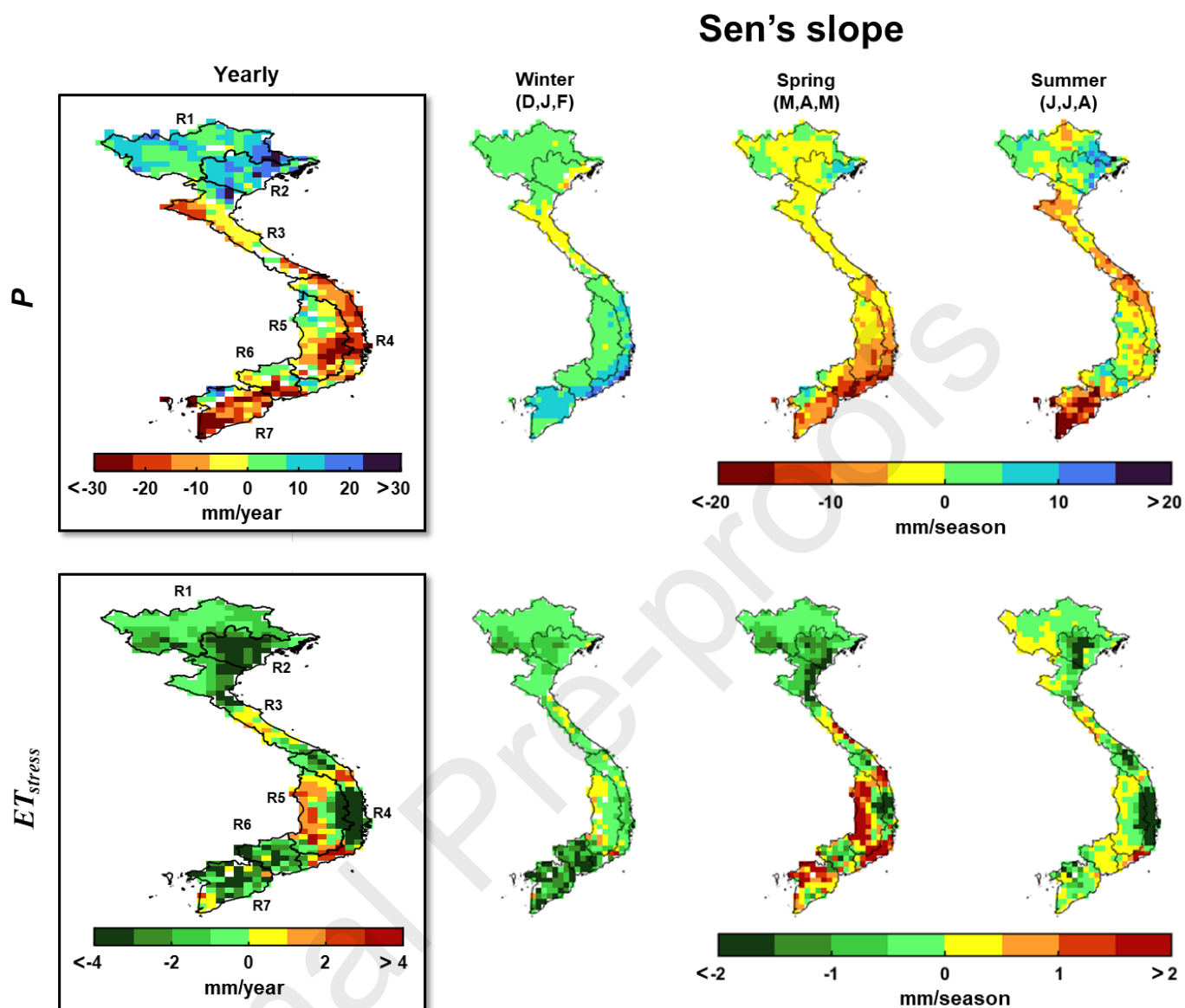
878 **Figure 1.** Land cover classification of the study region, geographic locations, altitudes, and
 879 annual variations in air temperature over the 18 ground stations used in the study.





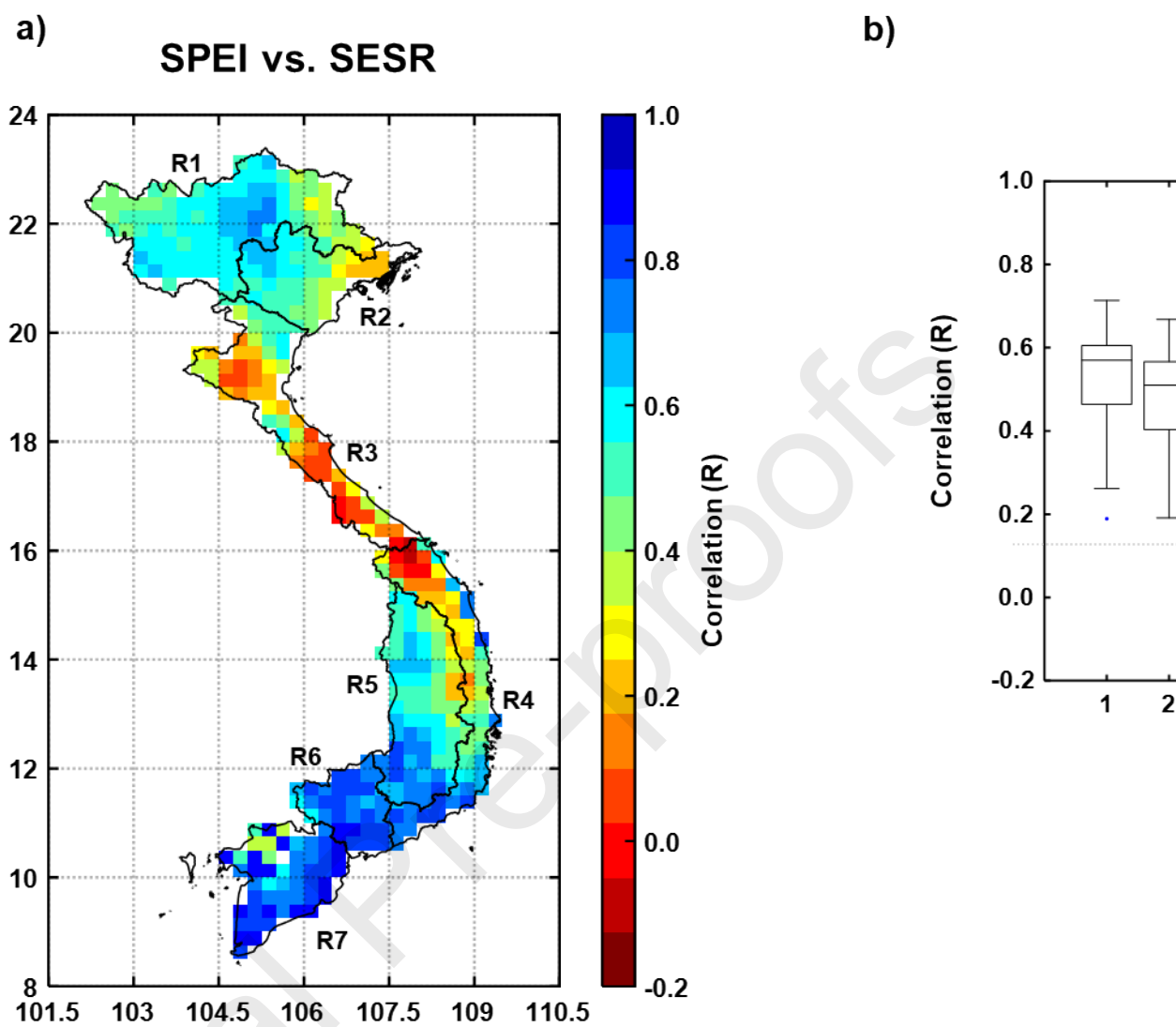
884

885 **Figure 3.** Mann-Kendall trend test of yearly and seasonal precipitation (P) and evaporative
 886 stress ($ET_{stress} = PET - AET$) during the study period (2003-2021) in Vietnam.



887

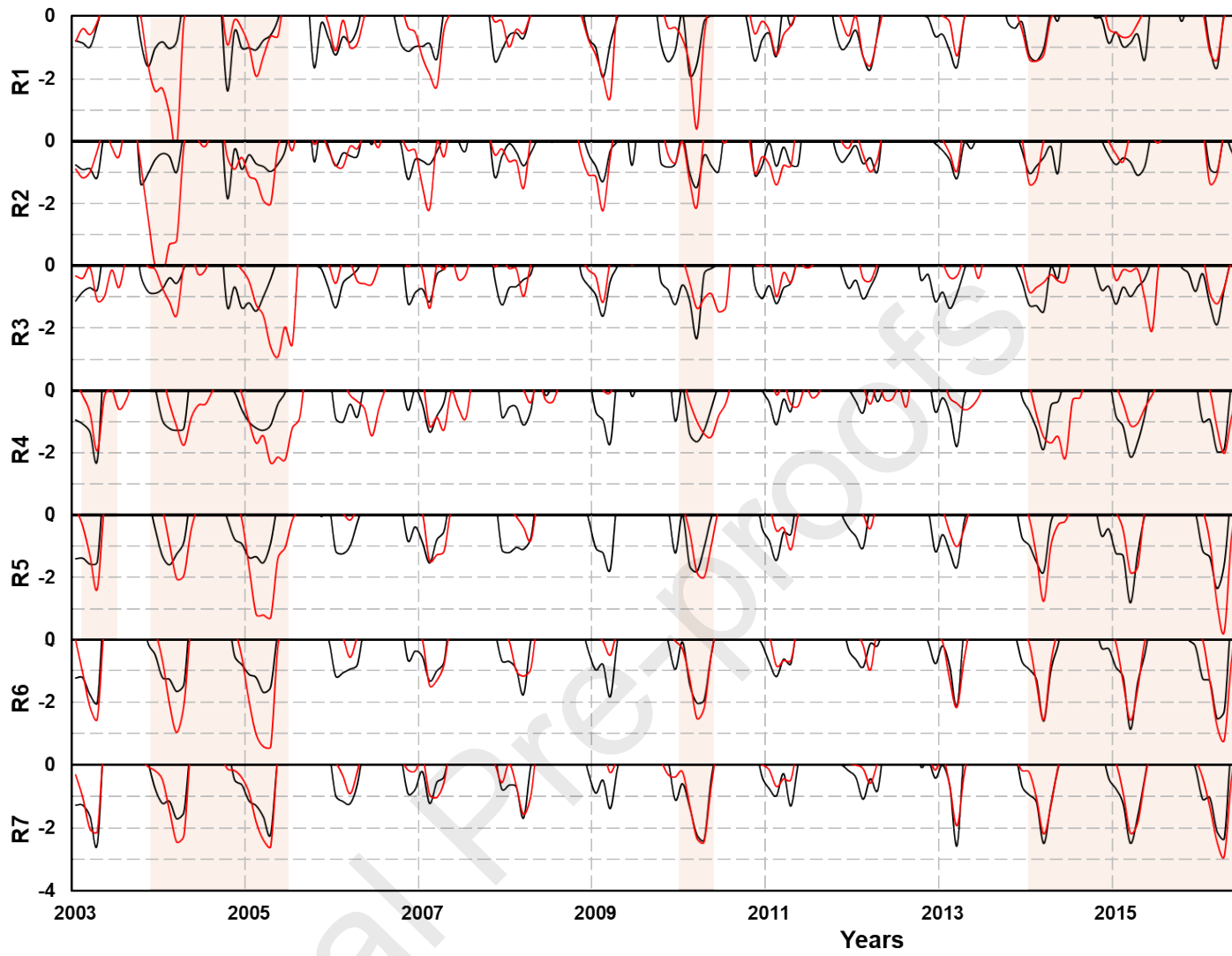
888 **Figure 4.** Sen's slope of yearly and seasonal precipitation (P) and evaporative stress
 889 ($ET_{\text{stress}} = \text{PET} - \text{AET}$) during the study period in Vietnam.



890

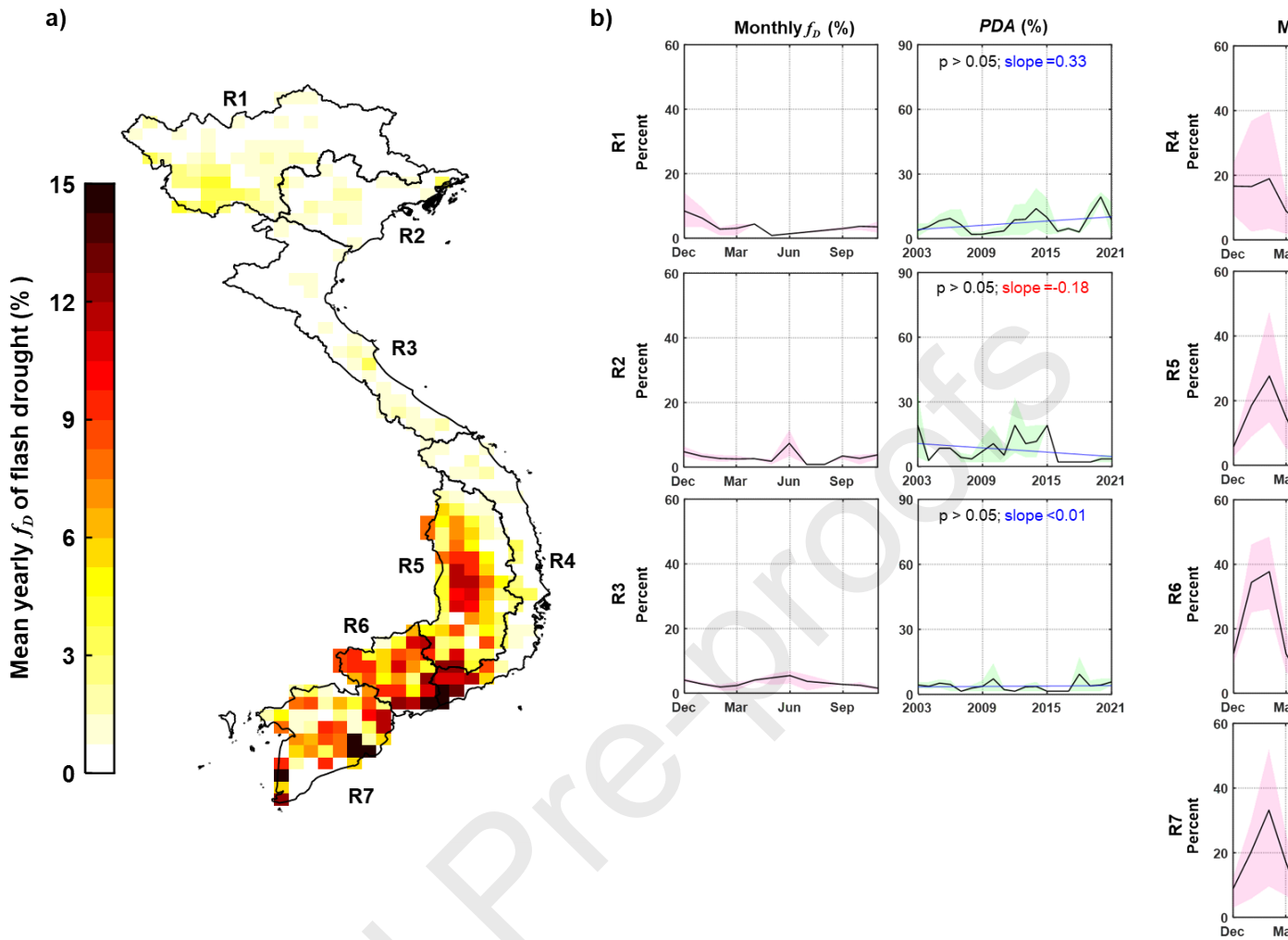
891 **Figure 5.** Distribution of temporal correlations between SPEI and SESR over Vietnam (a)
892 and boxplots for the seven sub-regions (b).

893



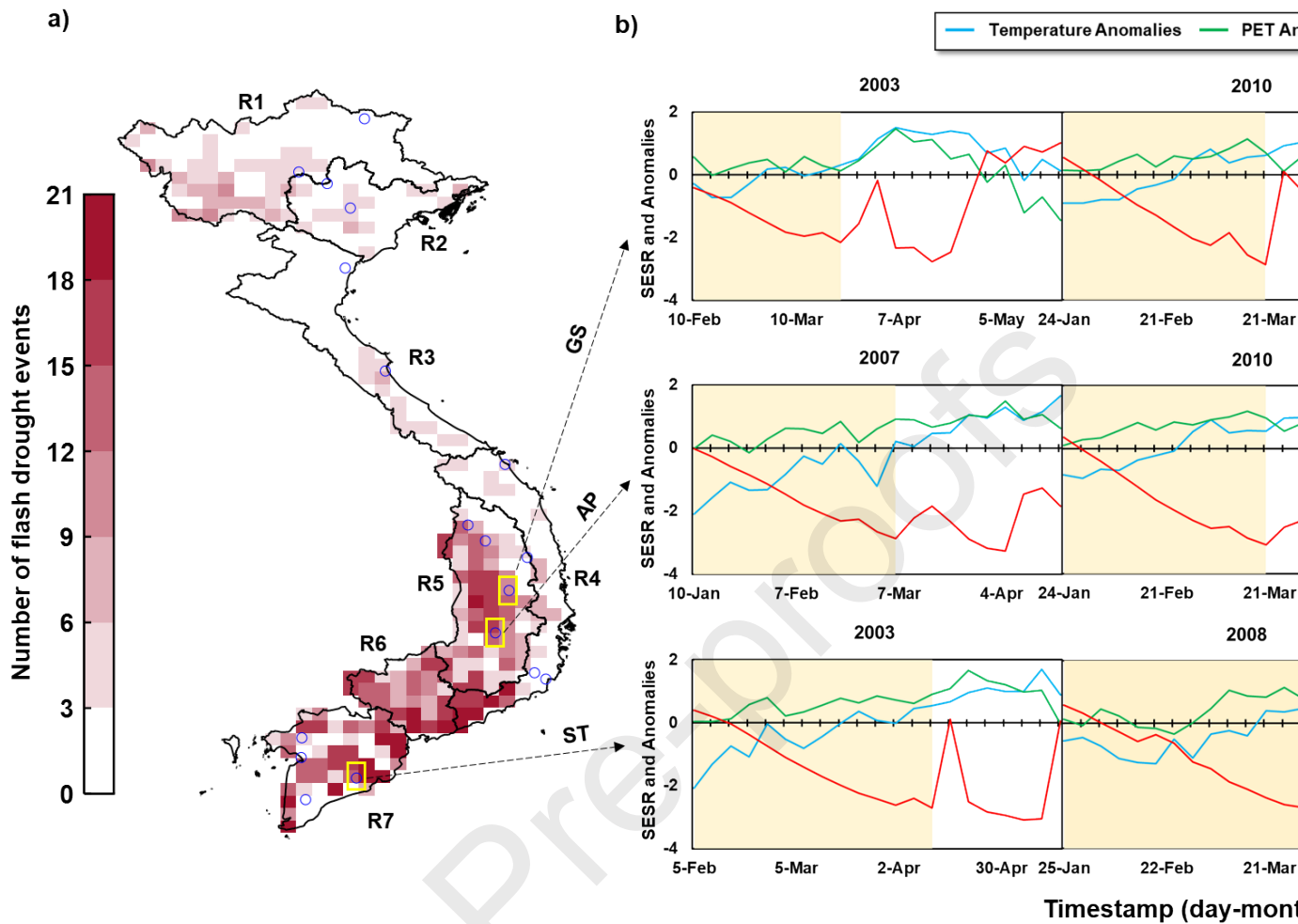
894

895 **Figure 6.** Temporal variations in monthly SPEI and SESR for the seven sub-regions during the
896 study period. Pink shades represent recorded historical droughts.



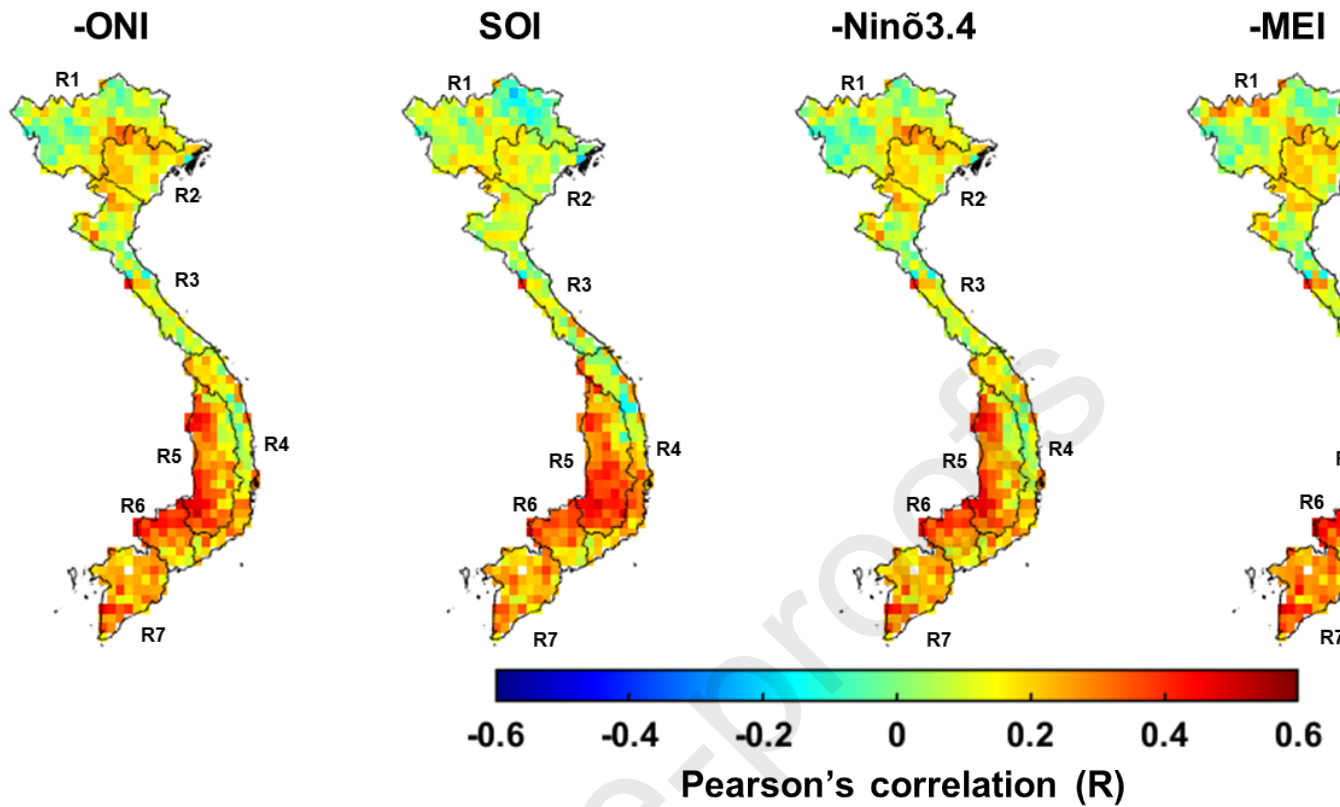
897

898 **Figure 7.** Flash drought occurrence in Vietnam and its characteristics: (a) mean flash drought
 899 frequency is shown as the percentage of years during the study period (2003-2021); (b) monthly
 900 frequency of flash drought occurrence (f_D) and flash drought area percentage (PDA) in the
 901 seven sub-regions during the study period. Black lines, blue lines, and light pink and green
 902 shading denote the mean values, trend lines, and ranges from the second quantile to third
 903 quantiles values, respectively. ‘Slope’ in blue and red represents increasing and decreasing
 904 trends, respectively; and ‘p-value’ in red and bold indicates the statistical significance.



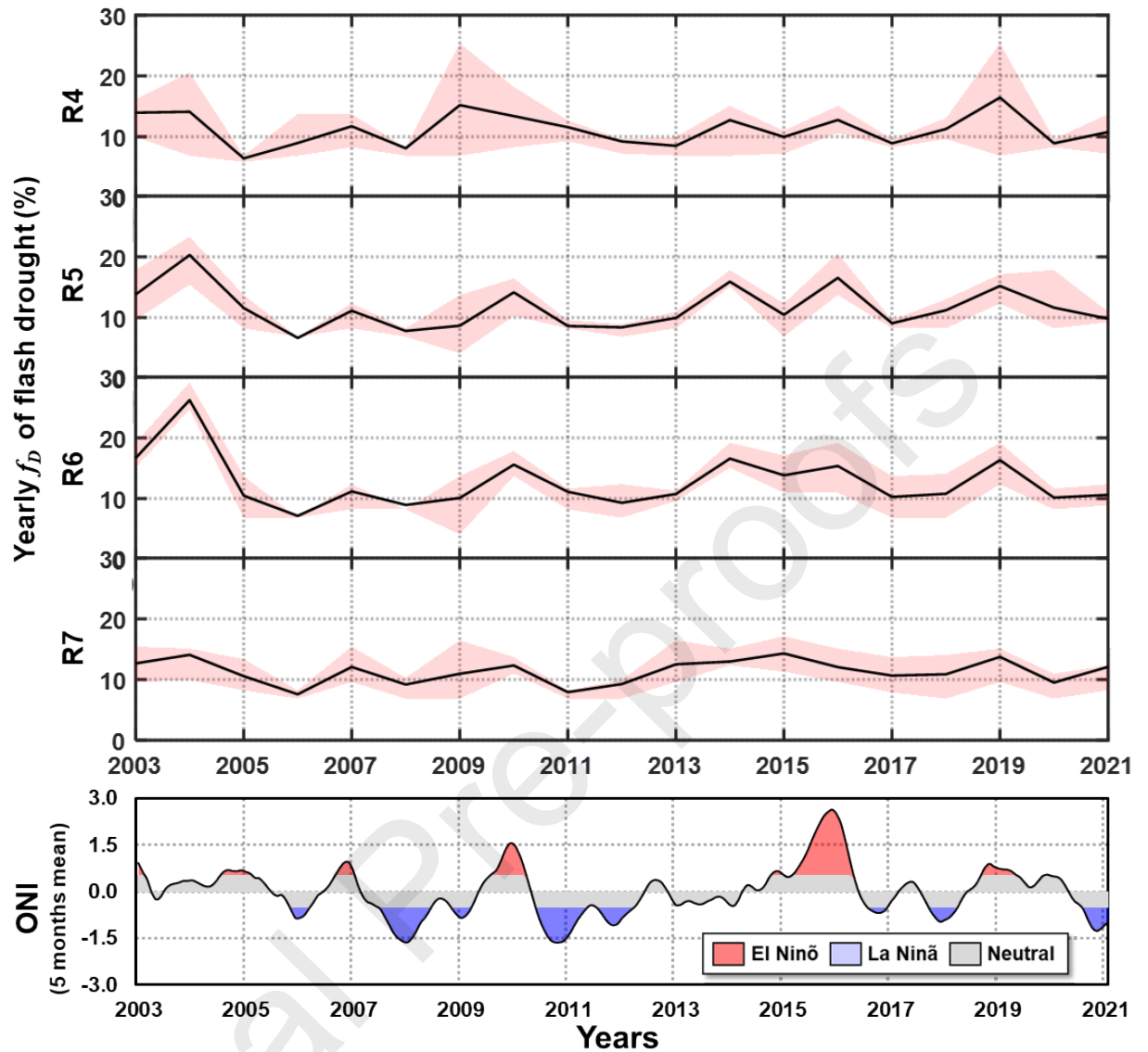
905

906 **Figure 8.** Flash drought occurrence in Vietnam and its drivers. (a) Number of flash drought
 907 events occurring during the study period (2003-2021). (b) Examples of the evolution of flash
 908 drought events (SESR-1 pentad) along with standardized air temperature anomalies and
 909 standardized potential evapotranspiration anomalies at three stations in areas with a large
 910 number of flash drought occurrences.



911

912 **Figure 9.** Pearson's correlations between the negative SESR and five climate variables at the
913 monthly scale across the study region. The signs of the ONI, Niño3.4, and MEI are reversed to
914 indicate El Niño and La Niña events in the same manner as the other indices.



915

916 **Figure 10.** Temporal variation between the yearly frequency of flash droughts in the four sub-
 917 regions (R4-7) with the highest occurrence rates and the Oceanic Niño Index.

918

919 **Table 1.** Dominant land cover and dominant climate types for each sub-region of Vietnam.

Sub-region	ID	Dominated land cover	Dominated climate type (ID)*
Northwest & Northeast	R1	Grasslands & Mixed Forests	Temperate, dry winter, hot summer (Cwa)
Red River Delta	R2	Croplands	Temperate, dry winter, hot summer (Cwa)

North Central Coast	R3	Cropland & Mixed Forests	Tropical, monsoon (Am)
South Central Coast	R4	Cropland & Mixed Forests	Tropical, savannah (Aw)
Central Highlands	R5	Cropland & Mixed Forests	Tropical, savannah (Aw)
Southeast	R6	Croplands	Tropical, monsoon (Am)
Mekong River Delta	R7	Croplands	Tropical, savannah (Aw)

920 *This information summarized in the Table is referred from [Beck et al. \(2018\)](#)

921

922

923

Highlights

- 924 • SESR might capture historical sustained drought events occurring in Vietnam.
- 925 • Flash drought had occurred over Vietnam during last two decades.
- 926 • The Northern Vietnam experienced fewer than 9 flash drought events.
- 927 • While Southern Vietnam suffered from 12 to 21 occurrence during study period.
- 928 • Vietnam flash drought has a relationship with ENSO climate phenomena.

929